Schlussberichte Juli 2003

Projekt
The Solar Production of Zinc

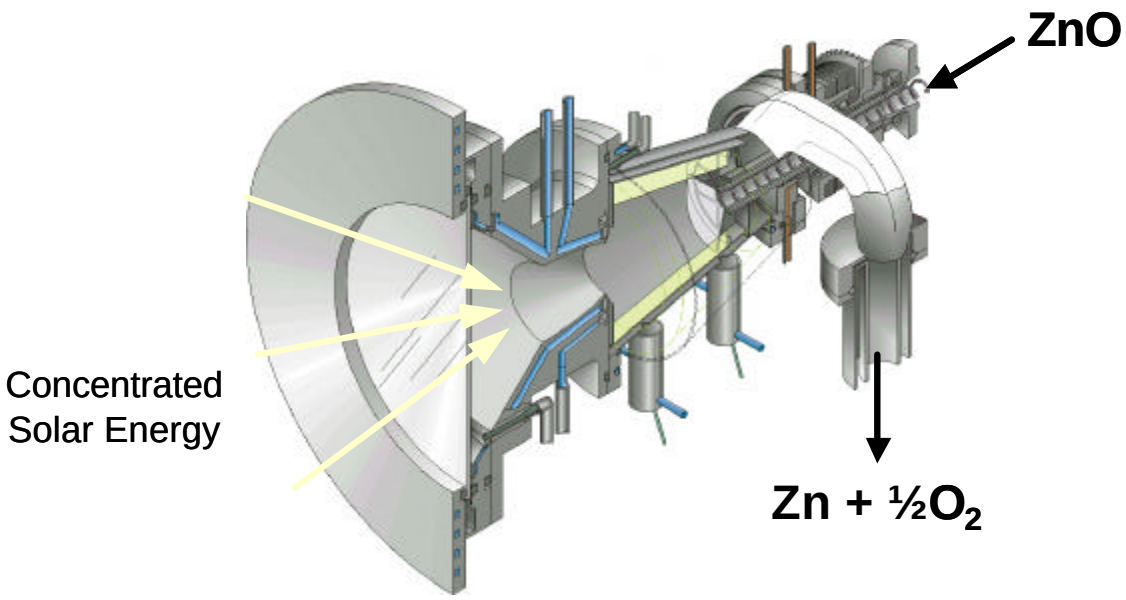

BFE OFEN UFE SFOE

Schlussbericht Juli 2003

Projekt
The Solar Production of Zinc

Autoren	Prof. Dr. Robert Palumbo and Prof. Dr. Aldo Steinfeld
beauftragte Institution	Paul Scherrer Institut
Adresse	CH-5232 Villigen PSI
Telefon, E-mail, Internetadresse	056 310 3504. Robert.Palumbo@psi.ch; aldo.steinfeld@psi.ch
BFE Projekt-/Vertrag-Nummer	36849/76551
Dauer des Projekts (von – bis)	Januar 2000 - Dezember 2002

ZUSAMMENFASSUNG

We developed and tested two 10-kW solar thermochemical reactors (SLOPE and ROCA) for the thermal dissociation of ZnO(s) to its elements at temperatures above 2000 K. Both reactors respect the transitory nature of solar energy: the reaction proceeds with minimal delay when the sun is available and the reactors withstand the thermal shocks that often occur under the severe environment of transient intense solar radiation. The ZnO(s) for both concepts is directly heated by concentrated solar energy. The ROCA reactor concept has been patented and selected for further development.

The SLOPE reactor was used to establish reaction kinetics of the thermal decomposition of ZnO at a nominal N_2 pressure of 1 bar within the temperature range of 1950-2400 K. Flash Assisted Multi-Wavelength pyrometry was used to determine both the hemispherical emissivity of ZnO and its irradiated surface temperature for a given solar flux during the kinetic study. The decomposition rate is described well by the equation $m = 1.4 \times 10^9 \exp[-328{,}500/(8.314\ T)]$ g $m^{-2}s^{-1}$. The uncertainty in the equation depends on temperature, but for temperatures near 2000 K it is ±70% at a 95% confidence interval. The emissivity of ZnO is 0.9 for temperatures above 1900 K. Numerical models that combine the reaction kinetics with heat transfer processes were developed which describe well the decomposition reaction both for a pellet of ZnO(s) and for the ROCA reactor. Initial experimental and numerical studies show that the reverse reaction: $Zn + 0.5\ O_2$ under certain conditions can be described by a numerical model that presumes the reverse reaction is rate limited by the mass transfer rate of the Zn and O_2 to the reactor wall. Good agreement between the model and the experiment exists when the gases move through the reactor in the laminar flow regime and when the wall and gas temperatures are below the decomposition temperature of ZnO(s) but above the condensation temperature of Zn.

We further developed the SynMet process technology for co-producing Zn and syngas by the combined ZnO-reduction and CH_4-reforming. An improved vortex-flow solar reactor was designed, fabricated, and tested at PSI's solar furnace in the temperature range 1380-1676 K and for an input solar power between 3.6 and 5.7 kW. The reactor and peripheral components, including the quartz window at the reactor's aperture, performed trouble-free under approximate steady state conditions. High degree of chemical conversion (maximum conversion of ZnO: 100%; maximum conversion of CH_4: 96%) and reasonable energy efficiencies (maximum thermal efficiency: 22%; maximum exergy efficiency: 7.7%) were obtained.

An economic evaluation of the 2-step water-splitting thermochemical cycle based on Zn/ZnO redox reactions predicts a unit cost of solar H_2 varying in the range 0.11-0.15 $/kWh, based on its LHV and a heliostat field cost at 50 to 150 $/$m^2$. Thus, the proposed cycle, if realized at an industrial scale, can be competitive with the electrolysis of water using solar-generated electricity.

BFE OFEN UFE SFOE

Projektziele

The goal of this project was to advance the science required for the design of high temperature solar thermal chemical reactors. Of particular concern was developing the know-how required for designing an industrial scale solar reactor that can thermally decompose ZnO into its elements at temperatures near 2300 K. The products, Zn and O_2 are to be separated with a rapid quench.

An industrial reactor respects the transitory nature of solar energy. This constraint implies that the reaction proceeds with minimal delay when the sun is available, and it implies that the reactor withstands the thermal shocks that often occur under the severe environment of transient intense solar radiation. Secondly, the reactor must function reliably, even though the reactants reach temperatures above 2000 K under flux conditions available in a typical solar furnace. Because it is estimated that the heliostat field will represent up to 40% of the capital cost of a solar plant, an industrially interesting reactor must have high exergy efficiency. We define this efficiency as,

$$\eta = \frac{\dot{m}_{ZnO} \cdot \left|\Delta G^0{}_{rxn}\right|}{\dot{q}_{solar}} \cdot 100\%$$

where ΔG_{rxn} is the Gibbs function for forming ZnO(s) at room temperature from the products leaving the reactor.

Durchgeführte Arbeiten und erreichte Ergebnisse

Historical Background

The direct solar thermal decomposition of ZnO to its elements has been described as an attractive process for the storage of solar energy [1-9]. In this process, concentrated sunlight provides high-temperature process heat for the endothermic reaction

$$ZnO(s) \xrightarrow{T>2000\,K} Zn(g) + \tfrac{1}{2} O_2 \,.$$

At temperatures near 2000 K, the reaction proceeds. Solar radiation is thereby directly converted into the chemical energy of Zn and O_2. To avoid their recombination at high temperature, the gaseous products can be separated by gas phase electrolysis or quenched [10-12, 1]. The solar energy stored in the condensed Zn phase may be used as the fuel in a fuel cell or battery. When H_2 is the desired fuel, it has also been suggested that the Zn be used to split water in an exothermic reaction. In either scenario, the ZnO is recycled to the solar furnace. The solar thermochemical cycle for Zn, H_2, and electricity generation is depicted in Figure 1.

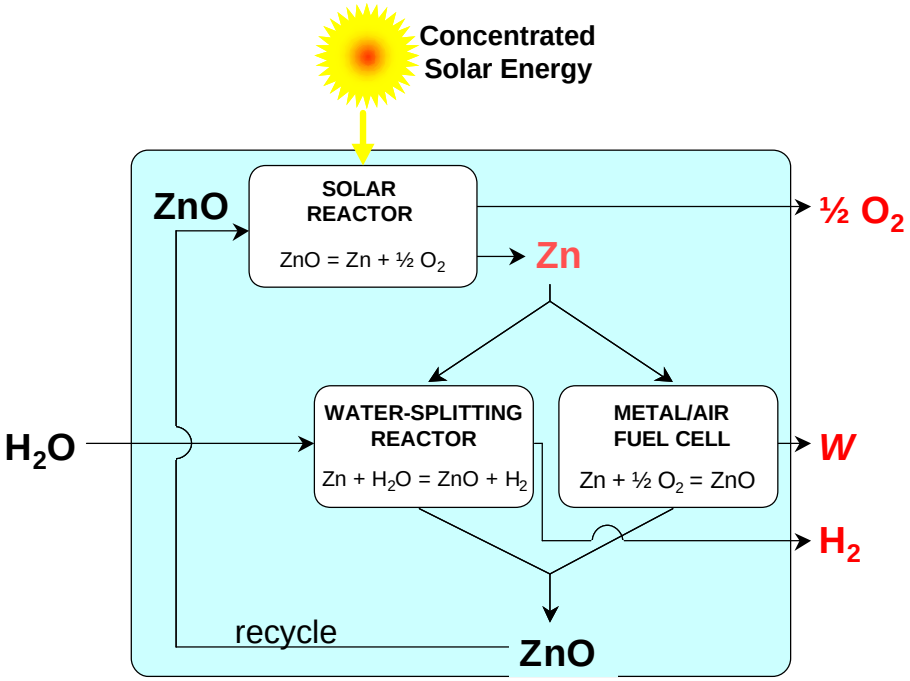

Figure 1: Schematic representation of the thermochemical cycle: In an endothermic, solar step, ZnO is thermally reduced into zinc and oxygen. Concentrated solar radiation is the energy source of the required high-temperature process heat. In an exothermic, non-solar step, zinc can either react with water to produce hydrogen or be used directly in a fuel cell or battery for generating electricity. In either case the resulting chemical product is ZnO, which is solar recycled. The net reaction is $H_2O=H_2+0.5O_2$; H_2 and O_2 are derived in different steps, eliminating the need for high-temperature gas separation.

At the start of this project, all of the work associated with a solar process for the thermal dissociation of ZnO was focused on the scientific frame work for the process: theoretical thermodynamic models of the process revealed the maximum exergy efficiency for decomposing ZnO; laboratory experiments were performed that verified Zn could be obtained at the exit of a solar reactor; numerical models were built to obtain first estimates as to how well the product gas mixture could be quenched. However, no one had reported on a reactor concept for effecting the ZnO decomposition; numerical models did not exist that described the potential performance of such reactors; and nothing was published on the mechanism of the Zn/O_2 recombination reaction. “The solar production of Zn” project was created as a step toward filling these voids.

General Description of Reactor Development Program

We designed, built, and tested two reactor concepts for the thermal dissociation of ZnO. The reactors were tested in PSI’s 45 kW solar furnace. They are known as Slope and ROCA. Condensed but specific descriptions of experimental set-ups are included in the results section of this report in order to facilitate the understanding of the results. In this section we describe generally the development of the reactors.

The Slope Reactor

Besides wanting a reactor with features of one scaleable to an industrial level, we wanted a reactor flexible enough for testing how best to keep the window clean of condensed products, we wanted a concept for establishing the decomposition kinetics of ZnO, and we wanted a concept for exploring how best to quench the product gases. In other words, we looked to develop a reactor

that is as much industrial in nature as it is an experimental research tool for our 45 kW solar furnace.

A schematic of the reactor that met these conditions is shown below (Figure 2). The reactor chamber (1) is partly filled with pressed ZnO powder forming a slope (2) with an inclination of approximately 45 degrees. The surface of the slope is directly irradiated by concentrated solar radiation entering through a quartz window (3). The uppermost ZnO layers are dissociated, whereas the non-reacted ZnO bed serves as insulation to protect the reactor walls directly in line with the concentrated sunlight. The walls are made from inconel. Those walls above and in front of the ZnO are lined with zirconia or alumina insulation. These surfaces receive the less intense emitted radiation from the ZnO surface. At the lower end of the slope (4), the non-reacted ZnO overflow is collected and recycled. The reactor can be operated both in batch and continuous modes with respect to the ZnO. In the latter case, solid zinc oxide particles are continuously fed into the reactor (5) and ripple down the slope, thus avoiding the need for a carrier gas. The transparent window is kept clean by several inert gas streams (6) which prevent zinc vapor from condensing on the quartz window. The gaseous reaction products and the inert gas flow continuously through the reactor to a chimney (7) and out to the quench unit.

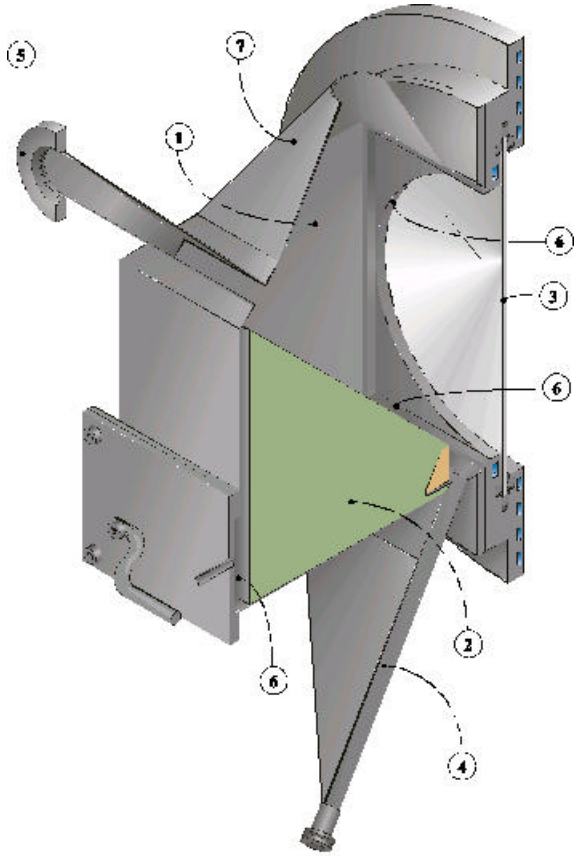

Figure 2: Schematic of a solar chemical reactor for the thermal decomposition of ZnO (SLOPE).

The ROCA Reactor

Figure 3 is a detailed schematic of the ROCA configuration. The main component is a rotating conical cavity-receiver (#1) made of Inconel steel that contains the aperture (#2) for access of concentrated solar radiation through a quartz window (#3). The solar flux concentration may be further augmented by incorporating a CPC (#4) in front of the aperture. Both the copper-made

window mount and the aluminum-made CPC are water-cooled and integrated into a concentric (non-rotating) conical shell (#5). The reactants are ZnO particles, which are fed continuously along the axis into the rotating cavity by means of a screw powder feeder located at the rear of the reactor (#6). The centripetal acceleration forces the ZnO powder to the wall where it forms a thick layer of ZnO (#7) that insulates and reduces the thermal load on the inner cavity walls. The gaseous products Zn and O_2 are swept out of the chamber by a continuous flow of inert gas that enters the cavity-receiver tangentially at the front (#8) and exits via an outlet port (#9) to a quench device (#10). The purge gas also keeps the window cool and clear of particles or condensable gases. With this arrangement, concentrated sunlight impinges directly on the top surface of the ZnO layer. This efficient heating condition leads to a system with a low thermal inertia and excellent thermal shock resistance. The ZnO serves simultaneously as radiation absorber, thermal insulator, and chemical reactant.

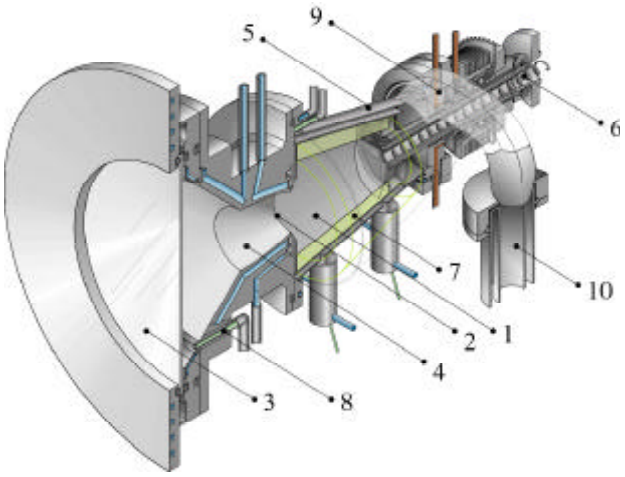

Figure 3: Schematic of a solar chemical reactor for the thermal decomposition of ZnO. 1= rotating cavity-receiver, 2 = aperture, 3 = quartz window, 4 = CPC, 5 = outside conical shell, 6 = reactant feeder, 7 = ZnO layer, 8 = purge-gas inlet, 9 = product outlet port, 10 = quench device.

Results

The Decomposition Kinetics of ZnO and First Steps toward a Heat Transfer Model

The Slope Reactor was modified slightly from Figure 2 during kinetic experiments. It was changed so that a ZnO pressed pellet could be located within the reactor at the focal point of PSI's 45 kW solar furnace. Section numbered (2) in figure 2 was replaced by a block of stabilized ZrO_2 insulation. In the center of the insulation, at the focal point of the solar furnace, a receptacle within the insulation block accepted the nominative 30 mm diameter 150 gram pre-sintered ZnO cylinder pellet. The front face of the cylinder was parallel to the reactor window. The experimental situation approached that of one-dimensional heat transfer along the pellet's axial direction.

The front surface temperature of the pellet was measured with the Flash Assisted Multi-wavelength Pyrometer developed in the Physical Science Group. The device also established the hemispherical emissivity of the ZnO. The mass of the ZnO pellet was measured before and after an experiment. The change in mass over the course of the reaction time divided by the irradiated surface area of the pellet determined the mass flux. The temperature measurement along with the mass flux rates were used to establish a quantitative expression for the decomposition rate of ZnO. In determining the rate expression, we assumed that the decomposition reaction took place on the irradiated surface of the ZnO.

We found that the decomposition rate is described well by the equation [13],

$$\dot{m} = 1.4 \times 10^{9} \exp\left(\frac{-328{,}500}{8.314\ T}\right) \text{ g m}^{-2}\ \text{s}^{-1}. \quad (1)$$

The uncertainty in the equation depends on temperature, but for temperatures near 2000 K it is ±70% at a 95% confidence interval. Details of the uncertainty analysis are found in Appendix A. The emissivity is 0.9 for temperatures above 1900 K.

Our kinetic expression differed from that of one published in the literature by Hirschwald [14]. As we expected, the major change between our kinetic expression and that found by Hirschwald was with regard to the pre-exponential term. Also as expected and in agreement with Hirschwald, we have an activation energy that is about 67% of the oxide's enthalpy of vaporization. Figure 4 shows the agreement between the experimentally measured decomposition rates and the calculated ones with the new kinetic expression. Also shown in this figure are the calculated rates using the kinetics described by Hirschwald.

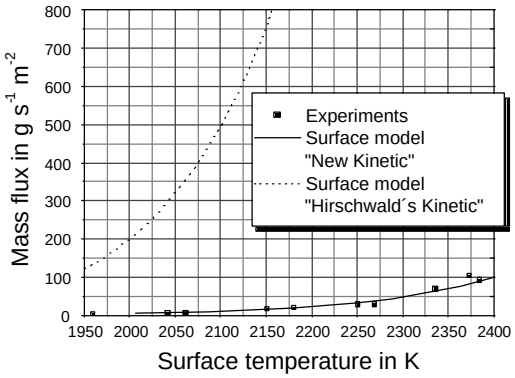

Figure 4: Comparison of measured and calculated mass flux as a function of temperature [13].

Furthermore, a one-dimensional unsteady and steady state heat transfer model that includes the physical processes radiation, conduction, and chemical decomposition was developed using the above expression for the reaction rate. The model predicts the measured steady state ZnO surface temperatures and the time to reach steady state. Figure 5 illustrates remarkable agreement between measured and calculated temperature profiles within and on the surface of the ZnO as a function of time [13]. (See Appendix B for Model discription).

In summary, this aspect of work done with "Slope" enabled us to obtain a good understanding of the physical-chemical properties of ZnO. We are now in a position to use this understanding to predict the performance of our ZnO reactors and compare our predictions with our experimental results.

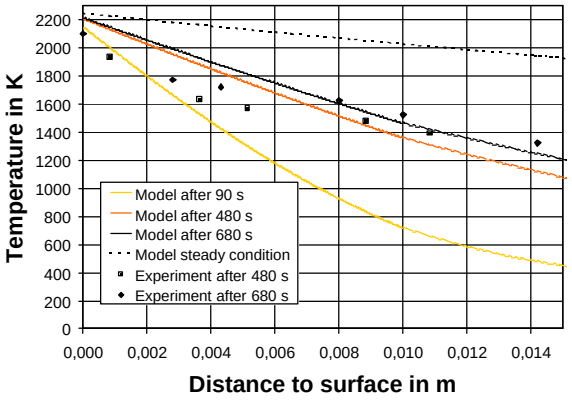

Figure 5: Measured and calculated temperatures vs. distance within ZnO solid for a solar flux of 170 W cm^{-2} [13].

The SLOPE Reactor as an Industrial Device for Producing Zn

This reactor was designed so that the reactants are directly heated by solar radiation. It was used in our solar furnace to decompose ZnO to its elements at temperatures ranging from 2000 K to 2400 K. The effective thermal inertial of the system is low: The ZnO surface temperature increased from 300 K to over 2200 K in a matter of seconds. The inconel reactor walls stayed well below their upper usable temperature limit of 1300 K. We thus conclude that the reactor concept adequately deals with the transitory nature of sunlight.

The direct heating condition introduced the challenging design requirement of keeping the window clean. We addressed the problem by developing a protective curtain of inert gas on the window. Finding the appropriate flow patterns and rates was determined experimentally. The details can be found in ref. [15].

Figure 6, however, gives some of the detail as to how the flow patterns were developed on the window. The manifold showing flows 1-3 is located at the bottom of the reactor and along the length of the window. The flow rates and orientations 1-3 were varied between experimental campaigns.

We learned that keeping the window clean requires controlling buoyancy driven flows near the window, avoiding flow induced pressure sinks near the window, and minimizing the pressure drop for flow through the reactor's chimney. Furthermore we were able to keep the window functionally clean for more than one hour of operation.

The qualitative fluid mechanics experimental studies led us to a solution for keeping the window clean for this particular reactor. The work, however, does not lead us to general definitive statements of how to keep windows clean for any reactor geometry, size, or chemically reacting system. More basic work is needed in the field of computational and experimental fluid mechanics before one could achieve such generality.

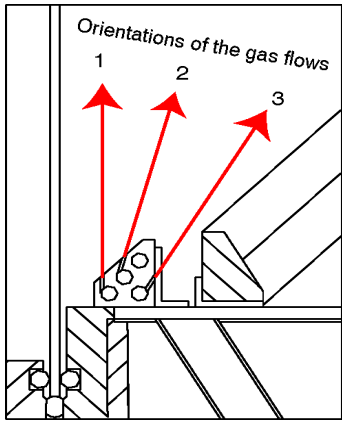

Figure 6: Orientation of gas flow in the SLOPE reactor. [15]

The ROCA Reactor as an Industrial Device for Producing Zn

A number of experiments were conducted with this reactor. Figure 7 is indicative of the reactor's thermal response [16].

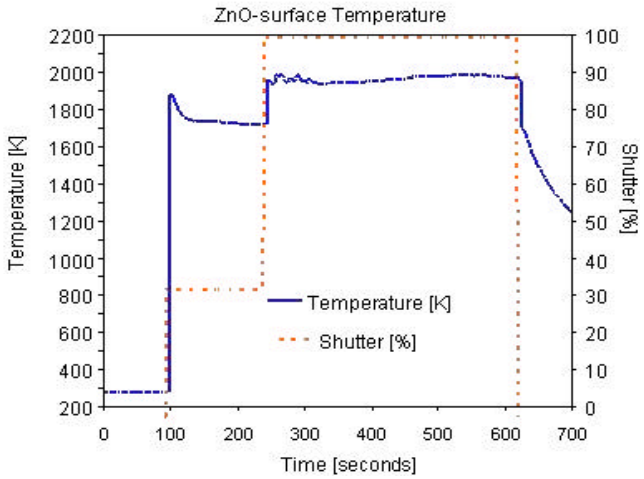

Figure 7: Solar cavity-receiver temperature during high flux solar irradiation. Solar input power was 6.3 kW with an average solar flux of 2228 kW m^2 over the aperture. Also plotted is the shutter position of the furnace. (100% = full power).

It is clear from the profile that the reactor has little effective thermal inertia: as soon as the furnace shutter is opened to 33%, the ZnO surface temperature increases at a rate greater than 1000 K s^{-1}. We also observed the immediate start of the reaction when the shutter was fully

opened, and the temperature at the conical shell did not exceed 900 K, corroborating that ZnO acts to some extent as a thermal insulator. In short, the reactor respects the transitory nature of sunlight and is constructed from conventional materials.

As mentioned above, our research effort with the slope reactor led us to a quantitative expression of the ZnO decomposition kinetics. Because the SLOPE reactor is not a cavity receiver, we carried out a number of experiments with a ROCA reactor in order to establish if the rate expression would hold under the geometric conditions of ROCA. In these experiments, pellets of ZnO with known starting mass and surface area were placed into a specific position within the ROCA cavity. The temperature was measured with a solar blind pyrometer. The mass changes on the pellets were established at the end of the experiment. The experimental reaction rate, the change in mass divided by the time of the run at the reaction temperature, was compared to calculated values using equation 1. Table 1 shows that the difference between the experimental and calculated values is within the uncertainty interval of the rate equation.

Experiment	Surface area ZnO sample in m^2	Reaction Temperature K	Reaction Time in seconds	Experimentally Measured Mass Change in grams	Calculated Mass Change in grams
March 6^{th} 2002	$7.00 * 10^{-3}$	1900	600	10.0	5.46
March 8^{th} 2002	$2.42 * 10^{-3}$	2125	1580	44.0	44.0
March 11^{th} 2002	$2.90 * 10^{-3}$	1790	1170	1.13	1.24
March 25^{th} 2002	$1.62 * 10^{-3}$	1950	1800	17.8	13.0
March 27^{th} 2002	$1.44 * 10^{-3}$	1890	1200	3.38	2.02
March 28^{th} 2002	$1.18 * 10^{-3}$	1980	1200	7.33	4.30

Table 1: Comparison between experimentally measured ZnO(s) mass change and the calculated mass change.

Because of this good agreement, we began the process of building a numerical model that linked the heat transfer processes to the chemical kinetics of the decomposition reaction for predicting reactor cavity temperatures and the exergy efficiency of the reactor for given solar flux inputs.

The details of the model can be found in ref. [17]. Here we present only a visual schematic (Figure 8) of how the model was built and the numerical results. Firstly the geometry of the reactor is defined with the inner portion of the reactor divided into a number of surfaces. Secondly, the model has two modules that interact with each other in an iterative manner. The module on the right establishes how the radiation is distributed within the cavity. The module on the left establishes how the absorbed radiation interacts with the cavity surfaces. Some surfaces may be reactants as is the case with the ZnO reactor described above. In this case, a portion of the energy is used to effect the ZnO decomposition reaction. Another part is conducted through the surface and out into the environment surrounding the cavity, a portion is convected away from the surface by any carrier gas that may be flowing through the reactor, and finally some of the absorbed energy is emitted from the surface as IR radiation. Because the energy distribution behind the surface and the radiation distribution on the surfaces are dependant on the unknown surface temperatures, the numerical solution to the energy distribution begins with a guess of the surface temperatures. Through an iterative process involving both modules which forces an overall energy balance on all surfaces, the cavity temperatures can be established for a given solar input.

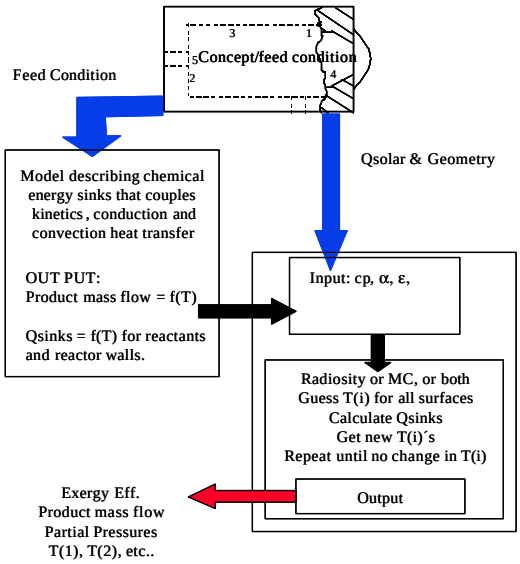

Figure 8: Schematic of the flow diagram for a general numerical model linking heat transfer and chemical kinetics. [17]

In order to make our first numerical estimates of the projected performance of the ROCA reactor, we prescribed an energy heat sink on surface 3 shown below in Figure 9. A finite difference model was used to establish a steady state heat sink as a function of temperature. Surfaces 2, 4, and 5, were presumed to be adiabatic. Surface 1 was given a radiosity value equivalent to the solar flux entering the cavity. The temperature of surface 6 was prescribed as 300 K. The radiosity exchange method with analytically determined and Monte Carlo determined view factors established how the radiation is distributed in the cavity. (This module could have used the Monte Carlo ray tracing method for the complete solution to the heat transfer problem.)

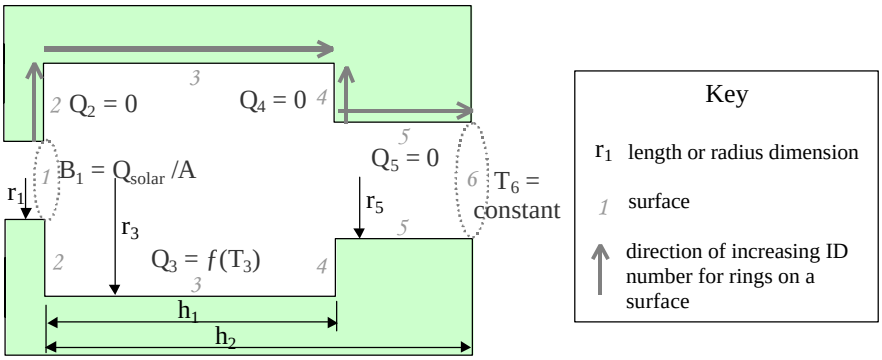

Figure 9: Model of ROCA reactor.

Figure 10 gives a portion of the numerical results for a 6.75 kW solar input through a 60 mm aperture. It is important to note, that they are ideal results in that several surfaces are considered as adiabatic and the heat sink on the reacting surface does not include convective heat transfer to a carrier gas flowing through the cavity. Thus they represent an upper limit on what one might expect for the performance of the ROCA reactor with this specific geometry and concentration ratio. On sees the estimated temperature distribution. The maximum wall temperature is 2020 K and occurs in the front quarter of the reactor. These temperatures lead to a Zn production rate of 0.16 g/sec. Using equation 1, the exergy efficiency is calculated as 11.2 %.

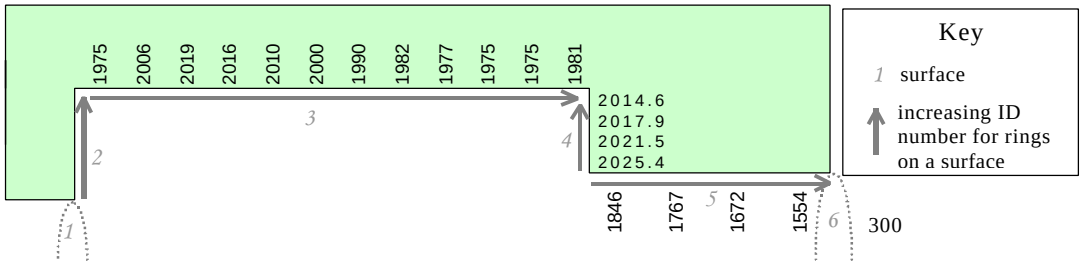

Figure 10: Calculated temperature distribution in ROCA reactor.

More modeling work is needed so that we describe even better the actual physical processes in the ROCA reactor. But one can argue these initial results suggest we have a good reactor concept for effecting the ZnO dissociation reaction: the Zn production rate and temperature distribution are reasonable for 6.75 kW solar input. The exergy efficiency is also reasonable for a small scale device: the average flux concentration ratio in the aperture was only 2400 suns and the hot cavity is exposed to a 300 K sink at the reactor exit where nearly 20% of the heat loss exits. When the concentration ratio is doubled the cavity temperatures increase by about 100 K and the exergy efficiency approaches 30%, an extremely good value for a small scale reactor.

We don't yet have a complete validation of the above model, partly because we continue to improve it. But we conducted an experiment where we estimated the temperature distribution in the ROCA reactor while it was experiencing a similar power input as to that in the model. The following figure is a photograph of ZnO pellets that were placed in the ROCA reactor from the front to the back of the cavity. Pellet one was located at the front of the reactor cavity and number 6 was at the rear of the cavity. It is clear that the temperature could not have been uniform throughout the cavity. The measured temperature of pellet 2 was 1925 K. The temperatures were estimated for the other samples: the reaction kinetics described above was used along with the measured mass changes to estimate the temperatures. The front pellet temperature, which is located nominally at the location where we calculated a temperature of 2020 K, was estimated to be 2083 K. And the back pellet, located nominally where the calculated temperature is 1975 K, was estimated as 1870 K. Thus our first numerical model of ROCA predicts similar, but higher temperatures than experimentally determined ones. Both the experimental and the numerical work predict a temperature gradient within the cavity, but the measured one is steeper than the numerical value, a result that is not surprising given the assumption of an adiabatic wall at the rear of the reactor in the model. Although not a complete validation of our numerical model, these results add credence to the numerical predictions of reactor performance.

Figure 11: Experimentally determined temperature distribution in ROCA reactor.

It was never possible to experimentally estimate the exergy efficiency of the reactor, because we were unable to establish a good mass balance. We learned that a substantial amount of the gaseous products did not exit the reactor; they diffused into the ZnO(s) layer and into the insulation. This unexpected result has a serious consequence for the reactor concept: It will be necessary to find a material for the inner cavity that is nearly gas tight, on which a thin layer of ZnO(s) can be continually added to the reactor. The ZnO layer must be thin so that the temperature at the interface of the ZnO and the nearly gas tight material is essentially at the decomposition temperature. This requirement prevents the re-oxidation reaction from occurring within the reactor.

We did not develop a reliable system for both rotating the reactor cavity and feeding the ZnO particles continuously. These problems are not of a fundamental nature, but they must be resolved if the reactor is to be practically operational.

The Reverse Reaction

The Zn yield at the exit of a quench device depends on the cooling rate of the gases and the rate at which Zn/O_2 recombine to form ZnO(s): A high Zn yield implies that the products experience a temperature-time history in which they are quickly brought through high temperatures, where the oxidation reaction is important, down to low temperatures, where oxidation is not important, so that one avoids significant loss of Zn. The answer to the pertinent question, “Can a quench lead to high Zn yields?” depends on whether or not nature prescribes a cooling rate that is technologically possible. We thus need to know the rate of the recombination reaction before we can assess the potential of a quench.

In this study, we presumed that the Zn/O_2, reaction takes place heterogeneously. With this assumption, we studied the reaction at temperatures below the decomposition temperature of ZnO but above the condensation temperature of Zn. Thus the available surface on which the reaction could take place was essentially the wall of the reactor.

The $Zn+O_2$ reaction was studied in the nominal temperature range of 1100 -1275 K by vaporizing Zn(l) to Zn and then mixing the vapor with O_2 entrained in Ar. Figure 12 is a schematic of the set-up. The outer shell of the set-up is a 1 m long 60 mm diameter quartz tube that is mostly enclosed within two electric furnaces. A crucible filled with Zn is moved into the left portion of the quartz tube after the temperatures within the two furnaces are stable at the values desired for an experiment. Two streams of Ar, preheated to a desired operating temperature, enter the Zn vaporizing cham-

ber of the tube. One stream flows directly over Zn(l) and transports Zn to a mixing zone. The other Ar stream flows directly to the mixing zone.

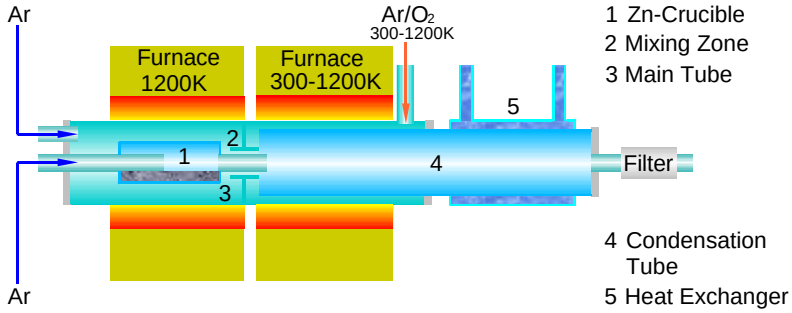

Figure 12: Schematic of the experimental set-up for studying Zn + O_2 reaction.

The mixing zone is located at the front of a second quartz tube, labeled the condenser. It is coaxial with the first tube. This second tube about 0.75 m long and 24 mm diameter extends from the entrance of the second furnace out beyond the furnace's exit. A mixture of Ar and O_2 is preheated as it flows within the annulus between the two tubes to the mixing zone. The second furnace sets the gas temperature for 0.3 meters of the condenser length. For the purpose of this investigation, we call this region the reaction zone. As the hot gas flows through the condenser, ZnO(s) can form on the wall. As the gas leaves the region enclosed by the furnace, it enters a zone where the condenser is cooled. Zn and ZnO(s) can form on the wall or on droplets of Zn or crystals of ZnO(s) carried in the gas. This entrained material is collected in a filter at the exit of the condenser tube.

The primary experimental variables were the molar ratios of Ar to Zn and O_2 to Zn, the total molar flow rate, the temperature of the reaction zone, and the duration of the experiment.

The Ar to Zn molar ratio was varied nominally from 50 to 250. These values were chosen, because we expect to see such ratios in the solar process. The ratio was always high enough to prevent Zn condensation in the reaction zone. The O_2 to Zn molar ratio was near 0.5 in order to best represent the products from the solar dissociation of ZnO(s). The flow rates were chosen so that the Re number within the reaction zone was nominally 50. Such a value served two purposes. Firstly, it enabled the velocity distribution at the entrance to the reaction zone to rapidly develop to the fully developed profile. Having a well-defined velocity profile over much of the reaction zone simplifies a mathematical description of the physical processes within this zone. Secondly, a low Re number flow means the gas in the entrance region has a significant radial velocity component. This flow situation helps insure good mixing of the gases near the center of the tube. The temperature range was bound by the upper limits of our furnaces and our desire to study the oxidation reaction at temperatures above the condensation temperature of Zn. A typical experiment lasted nearly 35 minutes. This timeframe insured that more than 90 % of the experiment occurred with constant and stable Zn flow rates. It also insured that we obtained measurable quantities of ZnO in the reaction zone.
At the start of an experiment, the condenser tube is weighed. At the end of an experiment, after the apparatus cools to room temperature, the tube is again weighed. The mass difference establishes the total amount of products deposited on the tube. The product distribution is also established within the reaction zone. 5 mm sections of the tube are cleaned and the tube is re-weighed after each cleaning, until the entire reaction zone is clean. This mass difference after each cleaning yields the amount of products that formed at a given location within the tube. The uncertainty in the mass measurements is ±2 % at a 95% confidence interval. The mass of the products that formed in the cold region of the condenser tube is also determined. These products are subjected to a quantitative X-ray diffraction analysis in order to ascertain the percentage of Zn within these products. The uncertainty in the Zn measurement is ± 10%.

We hypothesized that the oxidation reaction would occur on the wall of the reaction tube and be limited either by the rate at which Zn and O_2 diffused to the wall or by a chemical reaction rate. We further presumed that the chemical reaction rate is proportional to some power of the Zn and O_2 partial pressures, and is proportional to the wall's surface area. Working with each of these models, we looked to establish which hypothesis, if either, adequately describes the experimental observation.

We found that the formation of ZnO is best described by a model that presumes the rate of the Zn/O_2 is limited by the mass transfer of the two gases to the wall of the reactor.

We developed a model that presumes Zn and O_2 diffuses in the radial direction to the wall of the reaction tube on which the molecules react instantly to form ZnO(s). The bulk flow within the tube is assumed to be fully developed laminar flow. The model further presumes steady state radial mass transfer governed by Fick's Law for which the binary diffusion coefficients of Zn in Ar and O_2 in Ar are presumed to adequately describe the diffusion coefficients.

The physical situation is thus described by the following differential equation:

$$u_x \frac{\partial c_i}{\partial x} - D_{i-Ar}\left(\frac{1}{r}\frac{\partial c_i}{\partial r} + \frac{\partial^2 c_i}{\partial r^2}\right) = 0 ,$$

where i refers to either Zn or O_2; D_{i-Ar} is the binary diffusion coefficient of either Zn or O_2 in Ar; u_x is the axial velocity of the bulk gas flow at a given radius. It has the parabolic laminar profile; the values r and x are the radial and axial positions within the reactor tube: r =0 is at the tube centerline, and x = 0 corresponds to the axial position where the gases enter the reaction zone. The boundary condition at x = 0 and r > 0.003 m is $c_i = 0$; at x = 0 and $r \leq$ 0.003 m the condition is c_i = concentration of Zn or O_2 that existed in an actual experiment. The boundary condition at the wall is set by the assumption that the reaction Zn + $0.5O_2 \rightarrow$ ZnO(s) is infinitely fast. This constraint implies that at r = R, for at least one of the species, $c_i\big|_{r=R} = 0$, and

$$D_{Zn-Ar}\left.\frac{\partial c_{Zn}}{\partial r}\right|_{r=R} = 2D_{O_2-Ar}\left.\frac{\partial c_{O_2}}{\partial r}\right|_{r=R} .$$

The partial differential equation with the prescribed boundary conditions was solved using a finite difference numerical method with a 50 X 24 grid that covered the reaction zone. The number of grid points was increased until the change in the calculated amount of deposited ZnO was more than an order of magnitude lower than the uncertainty in the measurement of the deposited ZnO(s). In the development of the finite difference model, we evaluated the importance of axial diffusion and concluded that differences in our calculated values of deposited ZnO(s) with and without axial diffusion would be lower than the uncertainty in the measured amounts of deposited ZnO(s).

Table 2 shows the comparison between the amount of ZnO(s) recovered in an experiment in the reaction zone compared to the calculated amount based on the mass transfer model.

Experiment	Temp.[K]	n_{Zn}/n_{O2}	n_{Ar}/n_{Zn}	Tot.$ZnO_{exp.}$[g]	Tot.$ZnO_{mod.}$[g]	t[s]
1	1245	1.76	81	0.40	0.84	920
2	1250	1.03	139	0.25	0.49	920
3	1240	3.92	71	0.42	0.45	920
4	1245	1.59	90	0.40	0.62	920
5	1250	2.36	128	0.94	1.16	1920
6	1245	1.91	128	0.77	1.12	1920
7	1245	2.54	118	0.12	0.14	220
8	1160	1.19	252	0.39	0.70	1920
9	1200	3.04	128	0.55	0.92	1920
10	1110	1.46	282	0.41	0.66	1920

Table 2: The amount of ZnO recovered in the reaction zone and the amount predicted from a mass transfer model under various experimental conditions.

One sees good agreement between the calculated and recovered amounts of ZnO(s) for a variety of experimental conditions. Figure 13 also illustrates that the mass transfer model reasonably predicts the distribution of ZnO(s) throughout the reaction zone.

For these reasons we conclude that the re-oxidation reaction can be described as one which is limited by the mass transfer rate of Zn and O_2 to a surface when the gases are at a temperature far from the condensation temperature of Zn and are entrained in Ar and flowing through a reactor in the laminar flow regime. It is interesting to note that the model always over predicts the ZnO(s) deposition rate. We put forward two explanations, but prefer the 2nd because it also explains why the model over predicts the deposition in the first 4 cm of the entrance region of the reaction zone.

The model presumes an infinitely fast reaction, which of course is not possible. So the calculated deposition rate could be higher than the measured values for this reason. The model also does not account for the complex fluid flow condition in the first 4 cm of the reaction zone. Here the flow is a developing laminar flow. The large radial velocity components present in this region would tend to prevent Zn and O_2 from reaching the wall. In every comparison between an experiment and a calculation, we over predict the ZnO deposition rate in the hydrodynamic entry region. To quantitatively argue for one or the other explanation would require further development of the mass transfer model so that it accounts for the radial velocity field in the entrance region of the reaction zone.

Reference [18] gives a more complete development of the model. There one finds the impact of estimates of diffusion coefficients and estimates in measurement errors on the differences between the model and the experimental results.

Because our concern was to only establish a means for making reasonable estimates of the reverse reaction under the above specified conditions, we shifted our research to an important concern with regard to designing the solar reactor so that the highest possible Zn yields could be obtained.

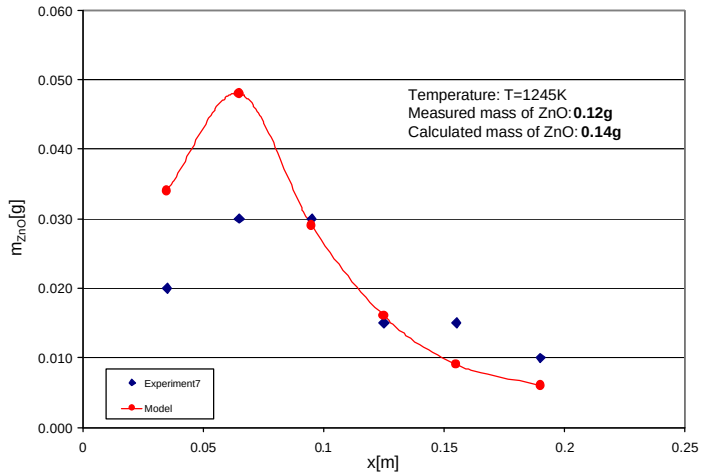

Figure 13: Experimental and calculated distribution of ZnO(s) on the reactor wall within the reaction zone. The experimental conditions correspond to experiment 7 in Table 2.

Given the experimental evidence supporting the notion that the Zn/O_2 reaction is likely a surface reaction, we suspected that the Zn yield exiting a solar reactor would tend to be higher if the carrier gas transporting the products out of the reactors hot zone were hot enough to avoid the condensation of Zn within the reactor in the zone where ZnO(s) is being dissociated. We speculated that Zn that condensed in this zone could lead to a large surface area on which the reverse reaction could take place. By suppressing the condensation of Zn in the high temperature region of the reactor, we hypothesized that all else being equal in the quench device, the Zn yield should improve. We thus conducted a set of experiments in the SLOPE reactor where we modified the reactor so that we could operate it with the Ar or N_2 carrier gas at elevated temperatures. Figure 14 summarizes our findings.

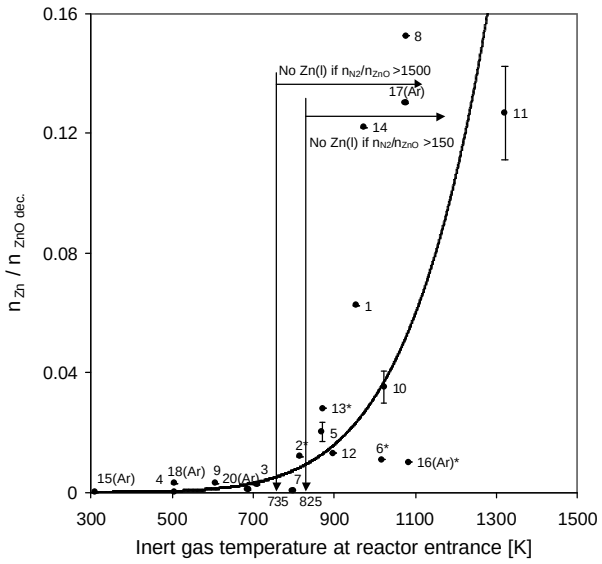

$nN_2/nZnO$	Experiment
150-460	1,11,12,13,14,16
500-950	3,4,5,6,7,15
950-1200	9,17
1300-1400	8
3000-4000	2,10,18,19

% Recovery of diss. ZnO	Experiment
60-70	1,2,3
40-60	4,5,6,7,8,9,12,15,16,19
20-40	14,17,18
0-20	10,11,13

Figure 14: Zinc yield from SLOPE vs. entrance gas temperature for various operating conditions.

The Zn yield is higher when we are able to keep the Zn from condensing in the hot zone of the reactor. Thus it an important design requirement for the solar reactor is to bring the carrier gas into the reactor at a temperature that avoids Zn condensation.

Co-Production of Zn and Syngas by the Combined ZnO-Reduction and CH_4-reforming Processes[1]

Zinc and synthesis gas (syngas), besides being important material commodities, are attractive as energy carriers. Zinc finds applications in Zn/air fuel cells and batteries, and it can also be reacted with water to form hydrogen [19] that can be further processed for heat and electricity. Syngas can be used to fuel high-efficient gas turbines and is also the building block of a wide variety of synthetic liquid fuels, including methanol - a promising substitute of gasoline for fuelling cars. However, the current industrial production techniques of both zinc and syngas carry severe environmental consequences. A recent life cycle analysis on the conventional fossil-fuel-based production of zinc by electrolysis and of syngas by natural gas reforming indicates total greenhouse gas emissions (GHG) of 2 kg $CO_{2\text{-equivalent}}$ per kg primary zinc and 0.8 kg $CO_{2\text{-equivalent}}$ per kg syngas, respectively [20]. These emissions can be reduced substantially, or even completely eliminated, by combining both the production of Zn and syngas and by replacing fossil fuels with concentrated solar energy as the source of high-temperature process heat. The proposed solar combined process, called “SynMet” [21,22], can be represented by the overall reaction:

$$ZnO + CH_4 \rightarrow Zn + 2H_2 + CO$$

The use of solar energy for supplying the enthalpy of the reaction upgrades the calorific value of the initial reactants by 39%. Thus, using the SynMet process, solar energy is converted into storable and transportable chemical fuels.

The chemical thermodynamics and kinetics for reaction above have been reported in several studies [8,21-23]. The reaction is highly endothermic ($\Delta H°_{1300\ K}$ = 446.6 kJ/mol) and proceeds to completion at temperatures above about 1300 K. Figure 15 shows the h-T diagram of the reaction. In previous projects a fluidized bed reactor and a vortex flow cavity reactor for the SynMet process had been designed and tested at PSI [21,24]. Conducting experiments with these reactors pointed out the feasibility of the solar driven ZnO reduction by CH_4. However efficiencies had been low due to the need for excess gas for fluidizing and feeding ZnO. The molar ratio of the reactants was up to $n(CH_4)/n(ZnO)=35$. Attempts to reduce the carrying flow to the stoichiometric amount resulted in plugging inside cavity and feeding system. These problems were overcome by the reactor development work described in the following section.

1 Work partially funded by the Baugarten Foundation.

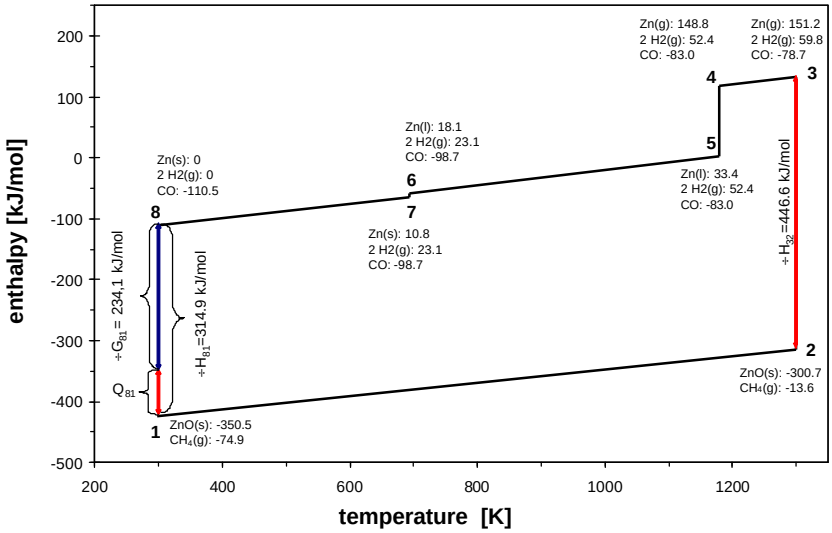

Figure 15: H-T diagram of the reaction ZnO + CH_4 → Zn + $2H_2$ + CO at 1300 K (1-2: heat ZnO and CH_4 from 298 K to 1300 K; 2-3: chemical reaction at 1300 K; 3-4: cool Zn(g), $2H_2$ and CO to 1180 K; 4-5: phase transformation Zn(g) → Zn(l); 5-6: cool Zn(l), $2H_2$ and CO to 692 K; 6-7: phase transformation Zn(l) → Zn(s); 7-8: cool Zn(s), $2H_2$ and CO to 298 K).

Methodology

Figure 16 shows schematically the new designed SynMet-reactor [25,26]. It consists of an insulated cylindrical cavity (length = 240 mm, diameter = 110 mm) that contains a 6-cm diameter windowed aperture to let in concentrated solar energy. The quartz window (diameter = 240 mm, thickness = 3 mm) is cooled and protected from condensable gases by an auxiliary gas flow. Both reactants CH_4 and ZnO are fed at ambient temperature. ZnO powder is continuously fed axially. Short pulses of CH_4 are simultaneously injected through a tangential inlet nozzle at the site where the ZnO particles fall. The result of the pulsed gas flow is the formation of a dense particle cloud that absorbs incoming solar irradiation efficiently and a decrease of the gas flow rate needed for distributing the ZnO in the reactor cavity compared to the former SynMet prototype [25]. The chemical products, zinc vapor and syngas, continuously exit the cavity via a tangential outlet port located at the front of the cavity, behind the aperture. The ceramic thermal insulation of the cavity walls has been further augmented to reduce conduction losses and allow for higher operating temperatures. Finally, the outlet port has been enlarged and insulated to prevent plugging by zinc condensation and to allow for a continuous mode of operation.

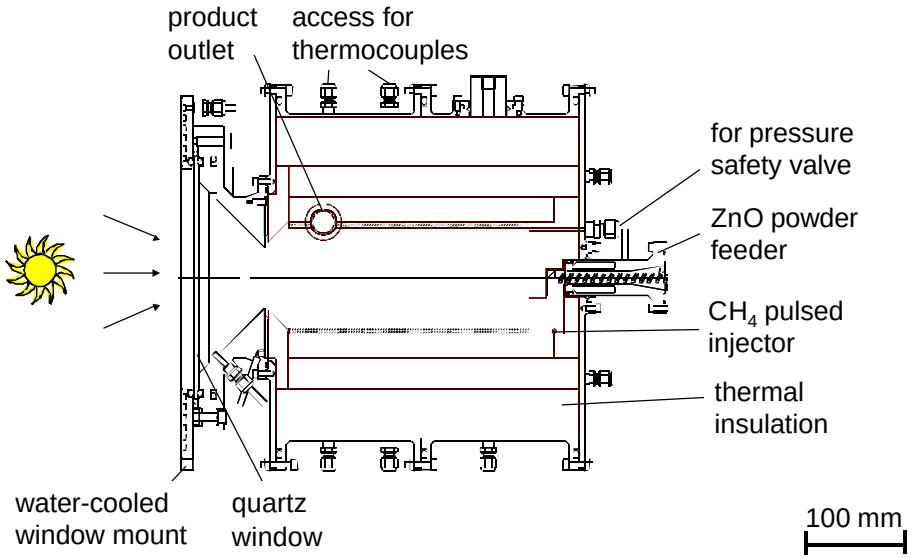

Figure 16: Scheme of the improved SynMet solar chemical reactor [26].

The solar experiments were carried out at the high-flux solar furnace of the Paul Scherrer Institute. The experimental set-up is shown in Figure 17. The ZnO powder is fed by a spiral-type feeder located at the rear end of the reactor cavity. A programmable logic module controls the pulse duration and the time interval between consecutive pulses of the CH_4 flow. In some experiments there was an additional CH_4 flow via a pipe positioned in the bottom of the rear section of the cavity. Reactor wall temperatures were measured with thermocouples type K and S inserted at the cavity wall but not exposed to the intense radiation. Furthermore the nominal cavity temperature was measured with a solar-blind pyrometer developed by IMPAC and PSI. This pyrometer is not affected by the reflected solar irradiation because it measures in a narrow wavelength interval around the 1.4 µm wavelength where solar irradiation is mostly absorbed by the atmosphere. The reactor's outlet gas temperature was measured by type K thermocouples. Pressure in the reactor is continuously monitored and restricted by a pressure safety valve. After exiting the reactor, the reaction products flow through a water-cooled Pyrex tube where part of the zinc condenses. A battery of particle filters collects the remaining solid products downstream. The gaseous products (CO, CO_2, CH_4 and H_2) are analyzed on-line by gas chromatography. The amount of zinc produced (or of ZnO reduced) is calculated by balancing the oxygen of CO, CO_2, and H_2O (H_2O is calculated by balancing CH_4 and H_2) contained in the gaseous products.

For verifying the Zn amount calculated from the oxygen in the gaseous products, additional experiments using a fixed bed of ZnO subjected to a continuous flow of CH_4 that was injected via a pipe positioned under the bed have been conducted. There was good agreement between the Zn amount calculated from the ZnO measured before and after the solar experiment and the amount calculated by balancing the off gas.

Representative product samples are taken from the material collected in the condenser and filters and are analyzed by X-ray diffraction.

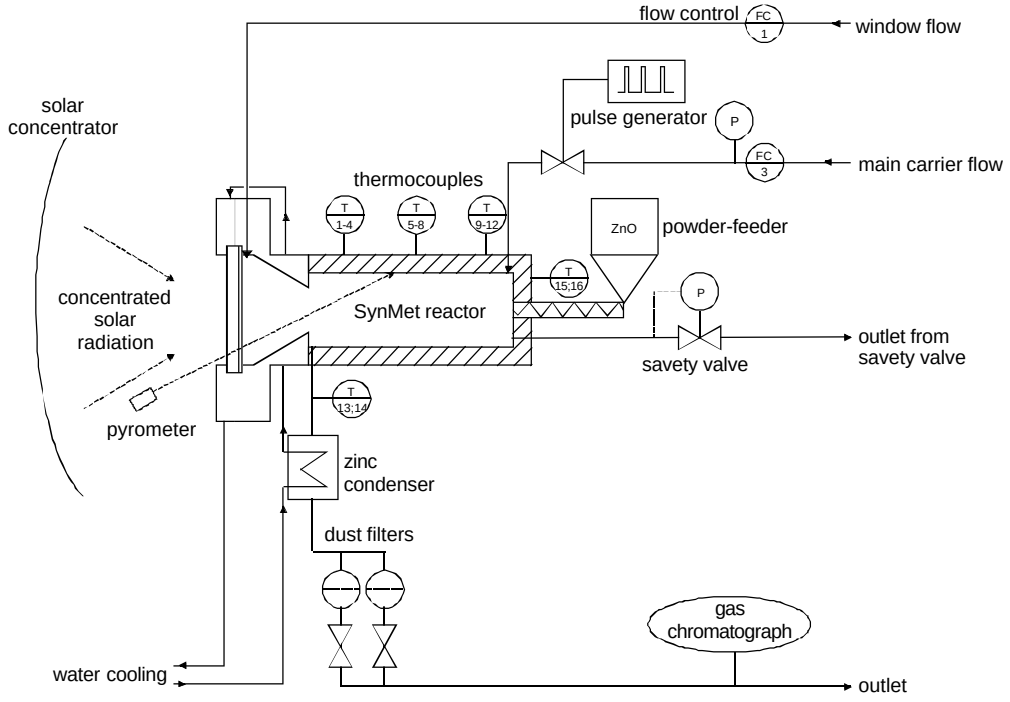

Figure 17: Experimental set-up at PSI's high flux solar furnace.

During a typical experiment the reactor is solar-heated to the desired temperature under a flow of N_2 and then isothermally subjected to the reacting flow. At the end of an experiment the solar radiation, the ZnO and CH_4 flow are cut off simultaneously and the reactor is cooled under N_2 flow. The duration of feeding lasted up to 33 min.

Results

Figure 18 shows the purity of Zn collected in the condenser and the filter as a function of nominal reactor temperature. The purity is increasing with increasing temperature. The mole fraction of Zn increased from 88% at 1300 K to 100% at 1500 K for the samples collected in the condenser and from 93% at 1300 K to 100% at 1370 K for the samples collected in the filter respectively. The degree of chemical conversion of CH_4 to syngas increased with temperature and reached 96% at 1676 K. Typical H_2:CO and CO_2:CO molar ratios in the syngas were in the range 1.5-3 and 0.08-0.25, respectively. Besides H_2 formation, CO, CO_2 and Zn, C, and H_2O were all produced during a solar experiment. The selectivity for the formation of H_2 decreased from 80% at 1300 K to 40% at 1676 K while selectivity for H_2O is increasing from 20% to 60 %. The selectivity for C and (CO_2) is decreasing from 48% (9%) at 1300 K to 37% (5%) at 1676 K while selectivity for CO is increasing from 43% to 58%. According to thermodynamic equilibrium calculations there should be either a composition with low amounts of H_2O and a large amount of C in case of $n(CH_4)/n(ZnO)>1$ or a composition with a large amount of H_2O and no C in case of $n(CH_4)/n(ZnO)<1$, but not a composition with both, large amounts of H_2O and C simultaneous. A feasible explanation could be the possible cracking of CH_4 to H_2 and C. Gaseous H_2 can react faster with the existing ZnO than C which has to be transformed into gas phase via Boudouard equilibrium.

The Zn production rate (Figure 19) increased with temperature for runs with pulsed CH_4 feeding. As expected in runs with pulsed CH_4 feeding and an additional CH_4 flow injected at the bottom of the cavity a favorable effect on the Zn production rate was observed. For the semi batch run with the fixed bed 11.5 g per min were obtained at 1550 K.

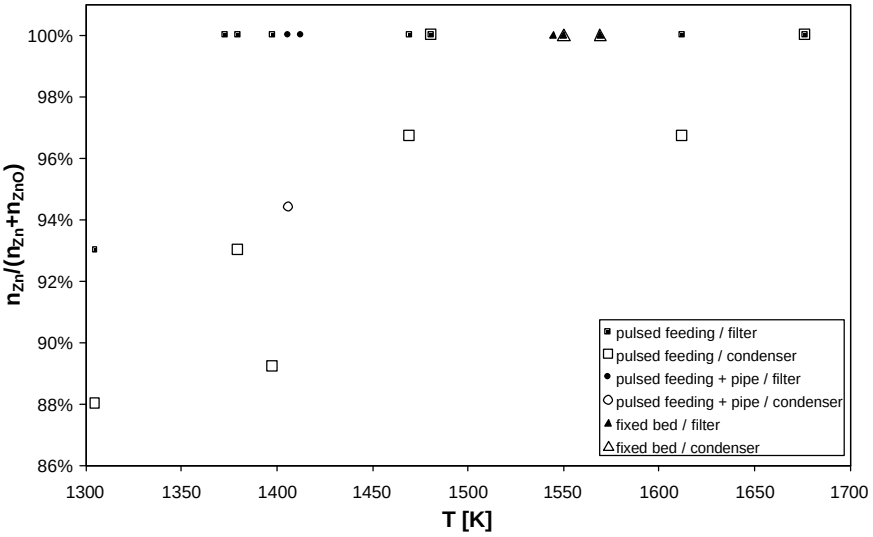

Figure 18: Purity of produced Zn.

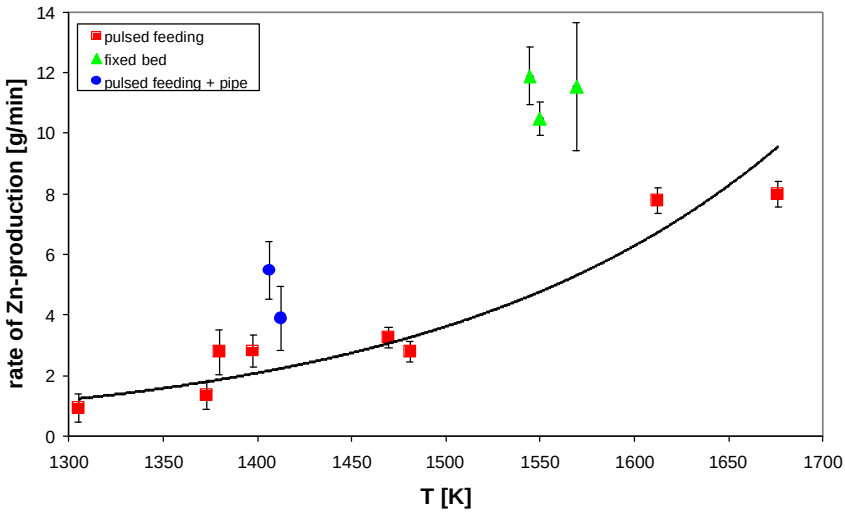

Figure 19: Rate of Zn production as a function of the nominal reactor temperature.

Figure 20 shows the energy balance of the reactor for different input solar power levels. Heat losses due to reflection and attenuation at the quartz window typically amount to 7 % of the solar power input. Conduction heat losses through the reactor walls vary between 20-30 % and re-radiation losses through the aperture vary between 20-30 % of the solar power input. The power

used for heating the reactants and N_2 to reactor temperature amounts to 5-11 % and that used for the chemical reaction amounts to 2.5-12 % for runs with pulsed feeding, 11 % for runs with pulsed and pipe feeding and 17 % for runs with fixed bed of the solar power input. Q_{other} includes the energy losses derived from thermal bridges and transients associated with heating the reactor's insulation. The thermal efficiency defined as the fraction of solar input power used for heating input flows to reactor temperature and driving the chemical reaction reached 9-25 %.

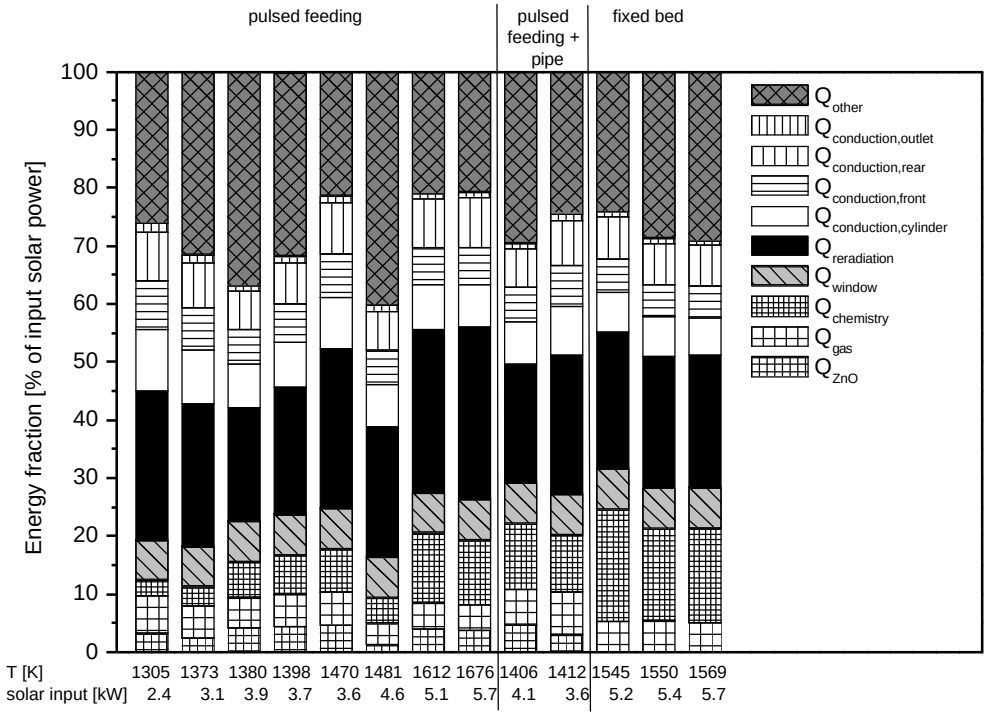

Figure 20: Energy balance of the reactor for the solar runs.

The thermal efficiency is defined as

$$h_{thermal} = \frac{n_{Zn} \cdot \Delta H^{\circ}_{\text{reactants@ 298 K} \rightarrow \text{products@T}_{\text{reactor}}}}{Q_{solar}}$$

where Q_{solar} is the solar energy input, n_{Zn} the amount of Zn produced, and ΔH^{o} the standard enthalpy change of the reaction when the reactants are fed at 298 K and the products are obtained at $T_{reactor}$. $h_{thermal}$ is shown in Figure 21. It increased with temperature and reached 22 % at 1612 K, but decreased for the run at 1676 K because of the almost complete conversion of CH_4. The exergy efficiency is defined as

$$h_{exergy} = \frac{n_{Zn} \cdot \Delta G^{\circ}_{\text{reactants@298K} \rightarrow \text{products@298K}}}{Q_{solar}}$$

where ΔG^{o} is the standard Gibbs free energy change of the reaction. As expected from the measured Zn production rates for runs II-VI (Figure 2), h_{exergy} increased with temperature and reached

5.4 % at 1676 K. It can be augmented by recovering the sensible and latent heat of the products. The highest exergy efficiency was 7.7%, obtained for the semi-batch run, pointing to the possibility of further increasing the amount of ZnO and CH_4 fed continuously for matching the reaction rate with the incoming solar power.

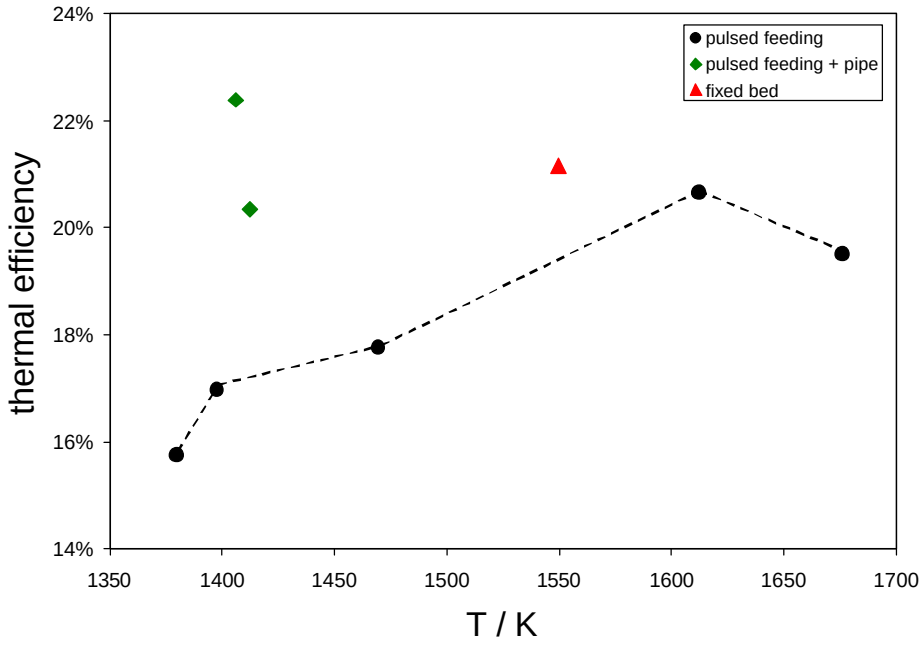

Figure 21: Variation of the thermal efficiency as a function of the nominal reactor temperature.

Economic Analysis of Solar Hydrogen Production

The cost analysis for solar hydrogen production via the 2-step water-splitting thermochemical cycle (see Figure 1) is carried out using the general procedure developed in [27], applied previously in the solar combined ZnO-reduction and CH_4-reforming [28]. The baseline operating conditions and enthalpy flows are the ones indicated in Table 1. The solar concentrating plant is assumed to be a solar tower system with a Cassegrain optical configuration of the type being developed at the Weizmann Institute of Sciences [29,30]. This innovative "beam-down" concentrating system uses a field of heliostats (two-axis tracking parabolic mirrors) to focus the sunrays onto a hyperboloidal reflector positioned at the top of the tower, which further re-directs the concentrated sunlight down to a CPC at the ground level. With this arrangement, concentrated solar radiation emerging out of the CPC (or an array of CPCs) can enter the solar reactor (or an array of solar reactors) located on the ground level, eliminating the need for massive and expensive tower, piping, and frequent personnel access to the tower top. The heliostat field is the largest single cost item in the solar plant. The assumed baseline cost of 150 \$/m^2 is consistent with current estimates of large-scale production of silvered glass heliostats [31,32]. The amount of area required is dependent on the efficiency of delivering solar heat to the receiver-reactor. The annual solar thermal efficiency, $h_{solar\ thermal}$, is defined as the fraction of annual solar radiation used for process heat. It is calculated, on a yearly basis, as the ratio of the enthalpy change of the reaction to the solar beam radiation incident over the heliostat area. Thus, $h_{solar\ thermal}$ is the product of the solar receiver's absorption efficiency, $h_{absorption}$, and the optical efficiency of the solar concentrating system, h_{optics}. The latter is assumed to be 58%, and is based on ray-tracing calculations that account for reflectivity, shading, alignment, and spillage losses due to geometrical and tracking imperfections [33]. The costs for the tower, tower reflector, and CPC were derived from [33], designed for a 34 MW_e solar-driven com-

bined cycle power plant. The cost of the receiver-reactor was based on judgment considering earlier data [33-35]. Costs associated with balance of plant were based mainly on [34] which displays detailed breakdowns of a variety of chemical systems. It includes site development, infrastructure, piping, instrumentation and control, security provisions, contingency, etc. The O&M cost is taken to be 2% of the capital cost. A fixed charge rate of 15% per annum is assumed, but early plants would probably have a higher fixed charge rate because of perceived high risk. The solar plant size is selected to be one that delivers 90 MW of concentrated solar power to the solar reactor, Q_{solar}. The only reason for this selection is that it allows the cost for the tower, tower reflector, and CPC to be directly extracted from [33] without inter/extrapolations. An important implicit assumption is that the solar tower technology becomes cost effective at large scales, but the question of the optimal size of the solar plant is not addressed in this analysis. Other baseline parameters are an annual beam irradiation of 2300 kWh_{th}/m^2/year and 2,300 equivalent full power hours per year (obviously intermittently). For all cases, the H_2 produced is assumed to have an energy content of 241 kJ/mol, which corresponds to its low heating value (LHV).

Government subsidies or any credit for CO_2 mitigation have been excluded from consideration. Credit for O_2 sale (O_2 derived from the solar reactor) has also been excluded. Also not accounted for is any cost incurred from storage and transport of reactants and products, and from transporting H_2 to the consumer site. Since the hydrolyser does not necessarily need to be located next to the solar plant, the transportation and storage costs for H_2 can be minimized or even completely eliminated if the hydrolyser is located next to the consumer site, but the transportation and storage costs for Zn and ZnO, which are comparable to those for coal, will then have to be added. The recycling of a quenching inert gas is not included explicitly in the cost breakdown, but its implications are discussed.

Table 3 shows the cost breakdown of the solar chemical plant and the unit cost of hydrogen, in US$/kWh. Included is also the cost of electricity generated using 70% efficient PEM fuel cells fueled by solar H_2. Calculations were carried out for two values of the solar concentration ratio: 5,000 and 10,000. As expected, the heliostat field causes the largest single cost item and is responsible for 44% of the total investment costs for the entire chemical plant. In contrast, the cost of the solar reactor represents only 13%. However, for a fixed product throughput, the solar reactor's efficiency dictates the size of the heliostat field (or, vice versa, for a fixed size of the heliostat field, the solar reactor's efficiency dictates the product throughput). Thus, reaching high solar reactor efficiencies and reducing the cost of the heliostats per unit area will have a significant impact on reducing the unit cost of H_2. For example, a reduction of the H_2 cost by 13% is possible for a heliostat field at 100 $\$/m^2$. The same magnitude of cost reduction can also be obtained by doubling the concentration ratio to 10,000 and, consequently, increasing the solar reactor's absorption efficiency by 23%. Note that doubling the concentration would require higher precision optics of the solar tower reflector and CPC, whose costs may double. It may also require more accurate heliostats arranged to have more ground coverage, resulting in higher blocking and shadowing and, therefore, higher costs per m^2 of heliostat field. Thus, the economical optimization of the solar flux concentration is a complex problem, not solved in the present study.

The specific cost of solar H_2 is estimated to be in the range 0.14-0.15 $/kWh (based on its LHV), assuming baseline parameters and a solar concentration ratio varying between 5,000 and 10,000. A sensitivity analysis for C=5,000 revealed that the cost of H_2 varies in the range 0.11-0.17 $/kWh when the heliostat field cost varies between 50 and 200 $\$/m^2$. This hydrogen cost has to be compared to that of hydrogen produced from water using other renewable energy based routes, e.g., solar, wind, biomass, geothermal, hydro, etc. The reference route is generally taken to be the production of hydrogen by electrolysis of water using solar-generated electricity. For solar thermal troughs systems (e.g. SEGS plant in California [36]), currently generating electricity at 0.12 $\$/kWh_e$, the reference cost of H_2 is cited as $0.20/kWh [36,37]. Thus, the proposed thermochemical route has the potential of becoming economically competitive. For wind electricity, currently at about 0.06 $\$/kWh_e$, the cost of H_2 by H_2O-electrolysis is estimated to be 0.17 $/kWh at present, and expected to come down to 0.10 $/kWh by the year 2005, as both the wind and electrolysis technologies mature [37]. It will be difficult for any solar technology to compete with the cost of H_2 from wind electricity unless the heliostat field cost drops under 100 $\$/m^2$ and the annual solar

thermal efficiency exceeds 40%. Obviously, for locations with rich solar insolation but poor wind resources, solar is going to be more competitive.

The cost of separating an inert quenching gas from the gaseous products exiting the solar reactor is not included in the cost breakdown of Table 2 because of the uncertainty regarding the need of such a quenching gas. However, if needed, it could play a decisive factor on the economics of the entire solar process. If N_2 were to be used as the inert quenching gas by a N_2/Zn dilution ratio of 10, the annual N_2 requirement would amount to about 9×10^6 kmol. Assuming current costs of N_2 production with membrane separation techniques at 0.06-0.08 \$/Nm^3 (by an electricity cost of 0.06 \$/kWh$_e$), the annual capital costs would be increased by 12 M\$, resulting in about doubling the specific cost of solar H_2 [38]. Thus, the economic feasibility of the proposed process is strongly dependent on the development of a Zn/O_2 quench technology (or, alternatively, in-situ Zn/O_2 electrolytic separation technology) that practically eliminates the need for an inert quenching gas.

The cheapest *non-renewable* H_2 is obtained at the moment via the catalytic steam-reforming of natural gas (with process heat supplied by the combustion of natural gas), at about 0.03-0.04 \$/kWh, assuming feedstock cost in the range 10-12 \$/MWh and excluding any externalities such as the cost of CO_2 mitigation and pollution abatement [39,40]. The external costs may be assessed with the help of a life cycle analysis (LCA) for evaluating the environmental burdens associated with the process by quantifying energy and materials used and wastes released during the entire life cycle. A LCA for the conventional syngas production indicates greenhouse gas emissions[2] of over 1 kg $CO_{2\text{-equivalent}}$ per kg syngas, of which 84% are derived from the combustion of natural gas in the endothermic steam-reforming step [20]. Once the external costs are *internalized*, the cost of solar H_2 is expected to become competitive with that of H_2 produced using fossil-fuel-based technologies.

The cost of electricity generated by H_2/O_2 fuel cells that are fueled with solar H_2 ranges between 0.31-0.33 \$/kWh$_e$, for the baseline case. This cost is not competitive against that of bulk electricity generated directly via solar thermal or even solar PV conversion systems, provided these systems are constrained to similar annual solar irradiation conditions of at least 2300 kW/m^2/yr with 2,300 equivalent full power hours per year. Thus, for large-scale stationary applications in regions of high insolation, direct solar electricity generation is clearly the preferable path, whereas for mobile applications it is obviously not a viable option. Solar thermal electricity systems can also feature on-site thermal storage capabilities (e.g. using molten salt as the heat transfer medium [36]) to allow for solar electricity dispatchability after sunset at more competitive prices than using chemical storage in the form of hydrogen. However, for regions having poor insolation, the cost of direct solar electricity generation often exceeds 0.30 \$/kWh$_e$. Transmission of solar electricity from regions of high insolation may be then a viable option; its cost will need to be compared with the cost of electricity from fuel cells fueled with solar H_2, including the additional cost of H_2 storage and transport. For mobile applications such as powering electric vehicles, fuel cells fueled with solar H_2 may compare favorably when judged against the alternative of using rechargeable batteries of similar performance and being charged with solar electricity. Furthermore, solar H_2 decouples the collection of solar energy and the generation of solar electricity, so that solar-H_2-fueled fuel cells can supply solar electricity around-the-clock to meet customer's energy demands whenever and wherever needed.

The weaknesses of this economic assessment are related primarily to the uncertainties in the viable efficiencies and investment costs of the various components due to their early stage of development and their economy of scale. The technical feasibility of large-scale windowed solar reactors, quenching techniques, and zinc hydrolysers needs demonstration. The solar tower-reflector + CPC technology also needs up-scaling to commercial size, but an alternative solar plant configuration with the receiver-reactor at the top of the tower could be developed.

---

[2] The three most relevant greenhouse gases were considered, namely: CO_2, CH_4, and N_2O. The amount of CH_4 and N_2O emitted over the entire process is converted into CO_2's equivalents (CO_2-equivalent) by using the Global Warming Potential factor of 21 for CH_4 and 310 for N_2O. A European electricity mix with 15% share of renewables and 32% share of nuclear was assumed in this study [20].

Plant size, energy, and mass flows		
Solar plant size (solar power input to solar reactor) [MW_{th}]	90	90
Solar input on heliostat field/year [MWh_{th}/yr]	356,896	356,896
Heliostat area [m^2]	155,172	155,172
Design ZnO/H_2O feed [kg-mol/hr]	398	398
Zinc metal production [tons/yr]	59,433	73,169
Hydrogen production [million-kWh/yr]	61	75
Electricity production [million-kWh_e/yr]	42	52
Efficiencies		
Solar concentration ratio, *C*	5,000	10,000
Optical efficiency of solar concentrating system, h_{optics}	58%	58%
Solar reactor's absorption efficiency, $h_{absorption}$	68%	84%
Cycle exergy efficiency, h_{exergy}	29%	36%
Fuel cell efficiency, $h_{F.C.}$	70%	70%
Annual solar thermal efficiency, $h_{solar\ thermal}$	40%	49%
Capital cost		
Heliostat field [M$, assuming \$150/m^2]	23.28	23.28
Tower [M$]	3.60	3.60
Tower reflector and CPCs [M$]	5.30	10.60
Solar receiver-reactor + periphery [M$]	7.00	7.00
Quencher [M$]	3.00	3.00
Hydrolyser [M$]	4.00	4.00
Balance of plant, indirects, contingency [M$]	8.90	8.90
PEM fuel cells [M$, assuming \$1500/kW_e installed]	27.48	33.83
Total for solar H_2 [M$]	55.08	60.38
Total for solar electricity [M$]	82.56	94.21
Specific installation cost for solar H_2 [$/kW installed]	2069	1843
Specific installation cost for solar electricity [\$/kW_e installed]	4506	4177
Annual cost		
Annual fixed charge rate [M$]	15%	15%
Capital cost for solar H_2 [M$]	8.26	9.06
Capital cost for solar electricity [M$]	12.38	14.13
O&M cost for solar H_2 [M$]	1.10	1.21
O&M cost for solar electricity [M$]	1.65	1.88
Total cost for solar H_2 [M$]	9.36	10.26
Total cost for solar electricity [M$]	14.03	16.02
Specific cost		
Unit cost of solar H_2 [$/kWh]	0.15	0.14
Unit cost of solar electricity from fuel cells [\$/kWh_e]	0.33	0.31

Table 3: Estimated costs of solar H_2 and of solar electricity generated by H_2/O_2 fuel cells fueled with solar H_2. The LHV for H_2 is assumed.

Publications

Peer-reviewed publications in *Science Citation Index* Journals

1. Moeller S., Palumbo R., “Solar Thermal Decomposition Kinetics of ZnO in the Temperature Range 1950-2400 K”, *Chemical Engineering Science*, Vol. 56, pp. 4505-4515, 2001.
2. Moeller S., Palumbo R., “The Development of a Solar Chemical Reactor for the Direct Thermal Dissociation of Zinc Oxide", *ASME - Journal of Solar Energy Engineering*, Vol. 123, pp. 83-90, 2001
3. Palumbo R., Keunecke M., Möller S., Steinfeld A., “Reflections on the Design of Solar Thermal Chemical Reactors: Thoughts in Transformation”, *Energy – The International Journal*, in press 2003.
4. Werder M., Steinfeld A., "Life Cycle Assessment of the Conventional and Solarthermal Production of Zinc and Synthesis Gas", *Energy - The International Journal*, Vol. 25, pp. 395-409, 2000.
5. Weidenkaff A., Reller A., Wokaun A., Steinfeld A., “Thermogravimetric analysis of the ZnO/Zn water splitting cycle”, *Thermochimica Acta* 359, pp 69-75, 2000.
6. Weidenkaff A., Reller A., Sibieude F., Wokaun A., Steinfeld A., “Experimental Investigations on the Crystallization of Zinc by Direct Irradiation of Zinc Oxide in a Solar Furnace”, *Chemistry of Materials*, Vol. 12, pp. 2175-2181, 2000.
7. Steinfeld A., Weidenkaff A., Brack M., Möller S., Palumbo R., “Solar Thermal Production of Zinc: Program Strategy and Status of Research”, *High Temperature Material Processes*, Vol. 4, Nr 3, pp. 405-416, 2000.
8. Palumbo R., Möller S., Steinfeld A., “Solar Thermochemical Processing: Challenges and Changes”, *High Temperature Material Processes*, Vol. 4, pp. 417-430, 2000.
9. Steinfeld A., “Recent Research Developments in Solar Thermochemical Processing”, *Recent Research Developments in Chemical Engineering*, Vol. 4, pp. 95-101, Transworld Research Network ISBN: 81-86846-63-8, 2000.
10. Steinfeld A., Epstein M, “Light years ahead”, *Chemistry in Britain,* Cover page & feature article, Vol. 37, Nr. 5, pp. 30-32, 2001.
11. Kräupl S., Steinfeld A., “Pulsed Gas Feeding for Stoichiometric Operation of a Gas-Solid Vortex Flow Solar Chemical Reactor”, *ASME - Journal of Solar Energy Engineering*, Vol. 123, pp. 133-137, 2001.
12. Weidenkaff A., Reller A., Steinfeld A., “Solar Production of Zinc from Zinc Silicate Ore Willemite”, *ASME - Journal of Solar Energy Engineering*, Vol. 123, pp. 98-101, 2001.
13. Kräupl S., Steinfeld A., “Experimental Investigation of a Vortex-Flow Solar Chemical Reactor for the Combined ZnO-Reduction and CH4-Reforming”, *ASME - Journal of Solar Energy Engineering*, Vol. 123, pp. 237-243, 2001.
14. Wieckert C, Steinfeld A., “Solar Thermal Reduction of ZnO Using CH_4:ZnO and C:ZnO Molar Ratios Less Than 1”, *ASME - Journal of Solar Energy Engineering*, Vol. 124, pp. 55-62, 2002.
15. Steinfeld A., “Solar Hydrogen Production via a 2-step Water-Splitting Thermochemical Cycle based on Zn/ZnO Redox Reactions”, *International Journal of Hydrogen Energy*, Vol. 27, pp. 611-619, 2002.
16. Kräupl S., Steinfeld A., “Operational Performance of a 5 kW Solar Chemical Reactor for the Co-Production of Zinc and Syngas”, *ASME - Journal of Solar Energy Engineering*, Vol. 125, pp. 124-126, 2003.

Chapter in Books and Editor of Books

1. Steinfeld A., Palumbo R., "Solar Thermochemical Process Technology", *Encyclopedia of Physical Science and Technology*, R. A. Meyers Ed., Academic Press, ISBN 0-12-227410-5, Vol. 15, pp. 237-256, 2001.

Ph.D. Theses

1. Stephan Möller, "Entwicklung eines Reaktors zur solarthermishchen Herstellung von Zink aus Zinkoxid zur Energiespeicherung mit Hilfe konzentrierter Sonnenstrahlung", Ph.D. Thesis ETH-Zürich Nr. 14277, 2001.
2. Anke Weidenkaff, "The Zn/ZnO Redox-Cycle for the Chemical Storage of Solar Energy", Ph.D. Thesis Nr. 13289, ETH-Zürich, 2000.
3. Kräupl S., "Chemische Speicherung von Sonnenenergie durch solares Reformieren von CH_4 mit ZnO", Ph. D. Thesis, No. 14744, ETH Zürich, July 17, 2002.

Peer-reviewed publications in Conference Proceedings

1. Kräupl S., Steinfeld A., "Pulsed Gas Feeding for Stoichiometric Operation of a Gas-Solid Vortex Flow Solar Chemical Reactor", *Proc. FORUM 2001 – ASME Solar Engineering Conference*, Washington DC, April 21-25, 2001.
2. Kräupl S., Steinfeld A., "Experimental Investigation of a vortex-flow solar chemical reactor for the combined ZnO-reduction and CH4-reforming", *Proc. FORUM 2001 – ASME Solar Engineering Conference*, Washington DC, April 21-25, 2001.
3. Kräupl S., Steinfeld A., "Operational Performance of a 5 kW Solar Chemical Reactor for the Co-Production of Zinc and Syngas", *Proc. ISEC'02 - ASME Int. Solar Engineering Conference*, Reno, April 17-19, 2002.
4. Steinfeld A., "From Solar to Chemical Energy", *Proc. Fuel Cell World*, pp. 356-366, Lucerne, July 1-5, 2002.
5. Palumbo R., Keunecke M., Möller S., Steinfeld A., "Reflections on the Design of Solar Thermal Chemical Reactors: Thoughts in Transformation", *Proc. 11th SolarPACES Int. Symposium on Concentrating Solar Power and Chemical Energy Technologies,* pp. 247-260, Zurich, Sept. 4-6, 2002.

Articles in Magazines and Newsletters

1. Steinfeld A., *SolarPACES News*, Issue 9, 2000.
2. "Fuel From Sunlight", *Vision – Science and innovation Made in Switzerland*, Vol. 4, p. 28, 2000.
3. Meier A., Palumbo R., Steinfeld A., "Chemische Brennstoffe aus Sonnenlicht", *MTZ-Motortechnische Zeitschrif*t, Nr. 3, pp. 242-249, 2001.
4. Meier A., Palumbo R., Steinfeld A., "Chemical Fuels and Materials from Sunlight", *MTZ-worldwide*, Nr. 3, pp. 15-19, 2001; and *5th Cologne Solar Symposium*, pp. 106-115, German Aerospace Center, Cologne, Germany, June 21, 2001.
5. Steinfeld A., "Langfristig Investieren", *Energie-Spiegel*, Nr. 5, 2001.
6. Steinfeld A., Hintermann A., "Sonnenenergie ist wandelbar", *ENET-News*, Nr. 52, 2002.
7. Steinfeld A., "Solar Approach Yields Synthetic Gas", *Fuel Cell Technology News*, Vol. 4, Nr. 9, 2002.
8. Steinfeld A., Meier A., Reller A., Hintermann A., "Konzentrieren und umformen", *ENET-News*, Nr. 53, pp. 10-11, 2002.

9. Steinfeld A., Meier A., “Die Kraft der Sonne”, *Bulletin ETH Zürich*, Nr. 287, pp. 16-19, 2002.
10. “Dall’energie solare a combustibili ecologici”, *Giornale del Popolo*, 22.11.2002.

List of Patents

1. Steinfeld A., “Process for the reduction of metal oxides”, Australia 59435/98.
2. Steinfeld A., Halmann M., “Verfahren zur thermoneutralen Reduktion von Metalloxiden zu Metallen durch gleichzeitige partielle Oxidation von Kohlenwasserstoffen”, Switzerland 1213/01, July 5, 2001.
3. Haueter P., Moeller S., Palumbo A., Steinfeld A., “Vorrichtung und Verfahren zur thermochemischen Behandlung von metal- und Kohlenstoffhaltigen Materialen unter Nutzung von externer Wärmestrahlung als Prozesswärme”, Switzerland Nr. 692 927, 13.12.2002.

Nationale Zusammenarbeit

The project was conducted in close collaboration with the ETH's Professorship of Renewable Energy Carriers (Head: Prof. Aldo Steinfeld) at the Institute of Energy Technology. The adjacent table lists the Diplom-/Semesterarbeiten conducted within the framework of this project.

		DIPLOMARBEIT	
1.	SS00	Bjorn Thorud	Verweilzeitverhalten im SynMet-Reaktor
2.	WS00	Marcel Beerli	Wirkungsgradberechnung eines chemischen Solarreaktors für die Zinkproduktion durch thermische Dissoziation von Zinkoxid
3.	SS01	Christian Cortina	Solar hydrogen by zinc hydrolysis
4.	WS01	Stefano Piffaretti	Zn quench by splash-condenser
5.	SS02	Javier Fernandez	Analyse der thermischen Dissoziation von ZnO zur Produktion von Zn in einem chemischen Solarreaktor
6.	SS02	Martin Seeman	Chemical Reactor Development for H2 Production by Hydrolysis of Zn
7.	WS02	Stephan Marty	Experimentelle Bestimmung der Wärmeleitfähigkeiten von Zinkoxid ZnO mit Kohle C, Kalkstein CaCO3 und Kalk CaO
8.	WS02	Enrico Tempesta	Wasserspaltung mittels Zink im Wirbelschichtreaktor
9.	WS02	Markus Schläpfer	Wasserspaltung mittels Zink im Wirbelschichtreaktor
10	WS02	Andreas Z'Graggen	Transient solution for an irradiated suspension of reacting particels

		SEMESTERARBEIT	
1.	WS00	Stefano Piffaretti	Wirtschaftliche Analyse eines Solar-Zink Kreislaufes für die Stromproduktion
2.	WS00	Gaetan Gogniat	Einfluss von Kaliumhydroxid auf der solaren Zinkoxid-Zersetzung mit CH_4
3.	WS00	Javier Fernandez	Zink/O2 Brennstoffzelle
4.	SS01	Nicola Ferretti	Solar reduction of ZnO with biomass
5.	SS01	Robert Macchi	Solar reduction of ZnO with biomass
6.	WS01	Rolf Fahrni	Overview of Hydrogen Production Methods and Costs
7.	SS02	Patrick Bürgi	Zink-Kondensation im Solaren Zink-Kreislauf - Experimentelle Untersuchung des Zink-Splash-Kondensators
8.	SS02	Andreas Z'Graggen	Modeling a solar cavity-receiver with selective window
9.	SS02	Paul Borer	Estimation of efficiency for various metal oxide/metal pairs in simplified solar thermochemical cycles
10	WS02	Alexander Heller	Temperature measurement in cavities by radiation py-

			rometer
11	WS02	Ly Hao	Design of an apparatus for the quantitative determination of metal yield from the products of the solar reduction of metal oxides
12	WS02	ThierryRöthlisberger	Thermogravimetry of ZnO+C process
13	WS02	Martin Renggli	Entwicklung eines Zink Sprinkler-Kondensators

Internationale Zusammenarbeit

Because of the high risk of the quench step in the pure solar decomposition of ZnO, we considered a solar carbothermic reduction. We were particularly interested in creating an EU project for which we would scale-up a reactor. During 2001 we successfully developed a joint European research project for this task. The project, called SOLZINC aims at scaling-up the chemical reactor technology for the solar production of Zn by carbothermic reduction of ZnO in a 0.5MW solar thermal input plant. Furthermore, the ZnO-Zn cyclic process encompassing the Zn-production solar plant combined with a Zn-air fuel cell will be developed to deliver solar electricity independent of location and time. The following table describes the project partners and their main tasks:

Partner	**Location/Country**	***Main* task** (partners are active in further tasks)
CNRS-IMP	Odeillo/ France	Administrative coordination, thermal and energetic diagnostic
PSI	Villigen/Switzerland	Scientific coordination, solar reactor design, buildup, test
ETHZ	Zurich/Switzerland	Solar reactor modeling and optimization: solar simulator
WIS	Rehovot/ Israel	Balance of plant for pilot Infrastructure: 1MW beam down solar concentrator
ScanArc	Hofors/Sweden	Zn-condensation (operation limits, pilot plant)
ZOXZY	Oberderdingen/ Germany	Zn-air fuel cell optimisation Treatment of spent cell products prior to reuse in solar plant

The key objective of SOLZINC is to develop and to experimentally evaluate a solar carbothermic ZnO-reduction process at the solar power input level of about 0.5 MW. In addition, the project includes the investigation of the material cyclic process and the interface of Zn-air fuel cells with the solar process.

This project was part of PSI's portfolio in the International Energy Agency's *SolarPACES* Program (Solar Power and Chemical Energy Systems – www.solarpaces.org). This IEA Agreement pursues the following objectives: 1) establish international collaborations and support research, development, and demonstration of solar thermal technologies for power and chemical applications; 2) support market development for the commercialization of these technologies; and 3) expand awareness of the potential of these technologies (including long term fuel supply). The participating countries are: Australia, Brazil, Egypt, EU, France, Germany, Israel, Mexico, Russia, South Africa, Spain, Switzerland, United Kingdom, and USA. Task and information sharing activities were established with leading SolarPACES research organizations, e.g. DLR (Germany), CIEMAT (Spain), CNRS (France), Weizmann Institute of Science (Israel), NREL (USA), SANDIA (USA), U. Colorado (USA), ANU (Australia), Tokyo Inst. of Technology (Japan), and private companies in the energy sector.

Bewertung und Ausblick

The research activity led to two reactor concepts for the direct thermal dissociation of ZnO, SLOPE and ROCA [15-16]. It is our opinion that the ROCA concept is at this time the one best suited for further development. Although SLOPE is a mechanically simple reactor concept: no moving parts and capable of operating in a batch or continuous mode, it is not a cavity receiver. This fact implies that the optical system delivering the light would need to be a field of mirrors with an extremely high optical quality that enabled the reactor without a CPC to receive sunlight at concentrations no less than 3000 suns. This technology does not exist. ROCA, on the other hand, is a cavity that can accept a CPC. The direct solar radiation on the reactants insures that the cavity has an excellent thermal response for Zn production. The cavity geometry can be designed for good conversion efficiencies of sunlight to chemical energy. However, a number of aspects of the ROCA reactor must be improved. Our plan for future work is given below.

During this research program, we established a quantitative kinetics expression for the thermal dissociation of ZnO(s) at temperatures in excess of 2000 K bracketed with an uncertainty interval at a 95% confidence interval [13]. For those interested in developing a reactor for the thermal dissociation of ZnO(s), the kinetic expression will allow one to estimate decomposition rates, temperature profiles, and sunlight to chemical energy conversion efficiencies for various reactor design concepts. The estimates are done by linking the reaction kinetics to the heat transfer processes occurring within the reactor. In this research program, we began developing a numerical method for making such a link.

The potential of separating the Zn from the O_2 with rapid cooling depends on the kinetics of the reverse reaction. We recognize this reaction as a surface reaction. In this study, we found that for gas temperatures above the condensation temperature of Zn but below the decomposition temperature of ZnO(s) the recombination reaction may be mass transfer rate limited. When the flow situation is laminar and the available surface for the reverse reaction is the reactor wall, we found good agreement between experimentally measured ZnO(s) deposit rates and rates calculated from a laminar flow mass transfer model. This finding represents a first step in being able to predict Zn yields in a solar reactor. One can use the mass transfer model, for laminar flow situations, to predict Zn loss in that part of the reactor where the temperature of the walls and gas are between the ZnO decomposition temperature and the Zn condensation temperature. The results from the studies in the Laboratory's Physical Science Group's current BFE projects, Zn Nucleation Project and the Zn Oxidation project, will enable us to describe the entire process by which Zn can be oxidized before exiting our solar reactor. When the entire process is quantified, we will be able to access the potential of quenching the gaseous products. In the mean time, it is clear also from our experimental studies that the inert gas entering the reactor should be at a temperature that prevents the condensation of Zn in the hot zone of the reactor.

We developed and investigated the SynMet process for co-producing Zn and syngas from the stage of a theoretical concept to a 5 kW laboratory reactor. This research includes both theoretical work e.g. thermodynamic computations and reactor modeling, and experimental work for developing and testing solar reactors. A vortex ZnO-CH_4 flow solar reactor was tested in the temperature range 1380-1676 K and for an input solar power between 3.6 and 5.7 kW. The reactor and peripheral components, including the quartz window at the reactor's aperture, performed trouble-free under approximate steady state conditions. High degree of chemical conversion (maximum conversion of ZnO: 100%; maximum conversion of CH_4: 96%) and reasonable energy efficiencies (maximum thermal efficiency: 22%; maximum exergy efficiency: 7.7%) were obtained. Higher energy efficiencies can be obtained by substituting the parasitic N_2 flow for CH_4 and by recovering the sensible and latent heat of the products.

From these activities, we obtained insight and understanding of the process. These insights were fundamental prerequisites for the discussion of a future scale-up of the reactor. The experimental results indicate that the solar chemical reactor technology can be further up-scaled and developed for an industrial application of ZnO-reduction combined with the reforming of natural gas. However as a result of our discussion we decided to scale up a process where a solid carbon source is used as reducing agent for ZnO (see SOLZINC project). Furthermore we developed important

know-how for solar chemical reactor designing and testing. This knowledge will be a basis for future solar chemical reactor developments.

An economic evaluation of the 2-step water-splitting solar thermochemical cycle (see Figure 1) predicts a unit cost of solar H_2 varying in the range 0.11-0.15 $/kWh, based on its LHV and a heliostat field cost at at 50-150 $/m^2. Thus, the proposed cycle, if realized at an industrial scale, can be competitive with the electrolysis of water using solar-generated electricity. The economic feasibility of the proposed solar process is strongly dependent on the development of an effective Zn/O_2 separation technique (either by quench or by in-situ electrolytic separation) that eliminates the need for an inert gas. Further development and large-scale demonstration are warranted.

The Swiss Federal Office of Energy (BFE) has agreed to support the follow-up project "Solar Chemical Reactor Engineering for the Solar Thermal Production of Zinc." The major focus of this new project will be to improve the ROCA reactor so that the limitations of the reactor concept described above can be removed. The project will have the following deliverables:

⇒ A 5-10 kW thermal input solar reactor for the thermal decomposition of ZnO.

⇒ Experimentally determined thermal performance map of the reactor as a function of solar input.

⇒ Numerical model that can predict reactor performance as a function of solar input.

⇒ Development of a non-solar reactor for producing H_2 from Zn and water vapor.

⇒ Papers that advance the scientific community's understanding of the industrial potential of a solar process for producing Zn from ZnO.

⇒ Papers that advance the scientific community's understanding of how to develop transient heat transfer numerical models that link radiation heat transfer with chemical reaction kinetics.

Referenzen

[1] Palumbo R., Lédé J., Boutin O., Ricart E. E., Steinfeld A., Möller S, Weidenkaff A., Fletcher E. A., Bielicki J. The production of Zn from ZnO in a high-temperature solar decomposition quench process—I The scientific framework for the process. Chemical Engineering Science 1998, 53 2503-2517.

[2] Fletcher E. A. and Noring J. E. High temperature solar electrothermal processing—zinc from zinc oxide. Energy 1983, 8 247-254.

[3] Fletcher E. A., Macdonald F. J., Kunnerth D. High temperature solar electrothermal processing II—zinc from zinc oxide. Energy 1985, 10 1255-1272.

[4] Palumbo R. and Fletcher E. A. High temperature solar electro-thermal processing III. Zinc from zinc oxide at 1200 - 1675 K using a non-consumable anode. Energy 1988, 13 319-332.

[6] Boutin O. Dissociation Thermique, suive de Trempe, de l'oxyde de zinc. Diplome d' Etudes Approfondies. LSGC-ENSIC, Nancy France 1996.

[7] Möller S. Untersuchung der solarthermischen Dissoziation von ZnO zu Zn und O_2 in einem Sonnenofen zur Speicherung von Sonnenenergie. Diplomarbeit, Universität Dortmund 1996.

[8] Steinfeld A., Kuhn P., Reller A., Palumbo R., Murray J., and Tamaura Y. Solar-Processed Metals as Clean Energy Carriers and Water-Splitters. Int. J. Hydrogen Energy 1998, 23 767-774.

[9] Bilgen E., Ducarroir M., Foex M., Sibieude F., and Trombe F. Use of solar energy for direct and two-step water decomposition cycles. Int. J. Hydrogen Energy 1977, 2 251-257.

[10] Weidenkaff A., Steinfeld A., Wokaun A., Eichler B., Reller A. The direct solar thermal dissociation of ZnO: Condensation and Crystallization of Zinc in the Presence of Oxygen. Solar Energy 1999, 65 59-69.

[11] Parks D. J., School K. L., and Fletcher E. A. A study of the use of Y2O3 doped ZrO2 membranes for solar eletrothermal and solar thermal separations. Energy 1988, 13 121-136.

[12] Fletcher E. A. Solarthermal and solar quasi-electrolytic processing and separtions: Zinc from zinc oxide as an example. Industrial and Engineering Chemistry Research 1999, 39 2275-2282.

[13] Moeller S., Palumbo R. Solar Thermal Decomposition Kinetics of ZnO in the Temperature Range 1950-2400 K. *Chemical Engineering Science*, Vol. 56, pp. 4505-4515, 2001.

[14] Hirschwald W. and Stolze F. Kinetics of the thermal dissociation of zinc oxide. Zeitschrift für Physikalische Chemie Neue Folge 1972, 77 21- 42.

[15] Moeller S., Palumbo R. The Development of a Solar Chemical Reactor for the Direct Thermal Dissociation of Zinc Oxide. *ASME - Journal of Solar Energy Engineering*, Vol. 123, pp. 83-90, 2001

[16] Haueter P., Moeller S., Palumbo R., Steinfeld A. The Production of Zinc by Thermal Dissociation of Zinc Oxide – Solar Chemical Reactor Design. *Solar Energy*, Vol. 67, pp. 161-167, 1999.

[17] Palumbo R., Keunecke M., Möller S., Steinfeld A., “Reflections on the Design of Solar Thermal Chemical Reactors: Thoughts in Transformation”, *Energy – The International Journal*, in press 2003.

[18] Keunecke M., Meier A., and Palumbo R. Solar Thermal Decomposition of Zinc Oxide: An Initial Investigation of the Reverse Reaction in the Temperature Range 1100-1250 K. *Chemical Engineering Science,* under review.

[19] Weidenkaff A., Reller A.W., Wokaun A., Steinfeld A. Thermogravimetric analysis of the ZnO/Zn water splitting cycle. *Thermochimica Acta*, Vol. 359, pp. 69-75, 2000.

[20] Werder M., Steinfeld A. Life Cycle Assessment of the Conventional and Solarthermal Production of Zinc and Synthesis Gas. *Energy - The International Journal*, Vol. 25, pp. 395-409, 2000.

[21] Steinfeld A., Frei A., Kuhn P., Wuillemin D. Solarthermal Production of Zinc and Syngas Via Combined ZnO-Reduction and CH_4-Reforming Processes. *International Journal of Hydrogen Energy*, Vol. 20, No. 10, pp. 793-804, 1995.

[22] Steinfeld A., Larson C., Palumbo R., Foley M. Thermodynamic Analysis of the Co-Production of Zinc and Synthesis Gas Using Solar Process Heat. *Energy - The International Journal*, Vol. 21, No. 3, pp. 205-222, 1996.

[23] Wieckert C, Steinfeld A. Solar Thermal Reduction of ZnO Using CH_4:ZnO and C:ZnO Molar Ratios Less Than 1. *ASME - Journal of Solar Energy Engineering*, Vol. 124, pp. 55-62, 2002.

[24] Steinfeld A., Brack, M., Meier A., Weidenkaff A., Wuillemin D. A Solar Chemical Reactor for the Co-Production of Zinc and Synthesis Gas. *Energy - The International Journal*, Vol. 23, No. 10, pp. 803-814, 1998

[25] Kräupl S., Steinfeld A. Pulsed Gas Feeding for Stoichiometric Operation of a Gas-Solid Vortex Flow Solar Chemical Reactor. *ASME - Journal of Solar Energy Engineering*, Vol. 123, pp. 133-137, 2001

[26] Kräupl S., Steinfeld A. Experimental Investigation of a Vortex-Flow Solar Chemical Reactor for the Combined ZnO-Reduction and CH4-Reforming. *ASME - Journal of Solar Energy Engineering*, Vol. 123, pp. 237-243, 2001

[27] Spiewak I. Introductory Guidance for Economic Evaluation of Solar-Thermal Power Plants. In: Roy A, editor. IEA Solar PACES, 1997.

[28] Steinfeld A, Spiewak I. Economic Evaluation of the Solar Thermal Co-Production of Zinc and Synthesis Gas. Energy Conversion and Management 1998;39:1513-18.

[29] Yogev A, Kribus A, Epstein M, Kogan A. Solar tower reflector systems: A new approach for high-temperature solar plants. Int J Hydrogen Energy 1998;23:239-45.

[30] Segal A, Epstein M. Comparative performance of “tower-top” and “tower-reflector” central solar receivers. Solar Energy 1999;65:207-26.

[31] Sanchez M, Romero M, Ajona J. Proc. 8th Int. Symp. Solar Thermal Concentrating Technologies, Cologne, Germany, Oct. 6-11, 1996;1:315-31.

[32] Science Applications International Co. Heliostat Manufacturing for Near-Term Markets. Phase I Summary Report, NREL-Contract ZAP-5-14168-02, 1996.

[33] Kribus A, Zaibel R, Carey D, Segal A, Karni J. A. Solar-Driven Combined Cycle Power Plant. Solar Energy 1998;62:121-9.

[34] Larson E.D., Katofsky R.E. Production of Methanol and Hydrogen from Biomass. Princeton University Center for Energy and Environmental Studies Report No. 271, 1992.

[35] Spiewak I, Tyner C.E., Langnickel U. Solar Reforming Applications Study Summary. Proc. 6th Int. Symp. Solar Thermal Concentrating Technologies, Mojacar, Spain, Sept. 28-Oct. 2, 1992;1:955-68.

[36] Tyner C.E., Kolb G.J., Geyer M, Romero M. Concentrating Solar Power in 2001 – An IEA/SolarPACES Summary of Present Status and Future Prospects. SolarPACES 2001.

[37] Glatzmaier G, Blake D, Showalter D. Assessment of Methods for Hydrogen Production using Concentrated Solar Energy, NREL/TP-570-23629, National Renewable Energy Labora-

tory, Golden, CO, 1998 (available From the National Technical Information Service, Springfield, VA 22161).

[38] Sturzenegger M. Private communication, 2001.

[39] Steinberg M., Cheng H.C. Modern and Prospective Technologies for Hydrogen Production from Fossil Fuels. Int J Hydrogen Energy 1989;14:797-820.

[40] Basye L, Swaminathan S. Hydrogen Production Costs – A Survey, DOE/GO/10170-778, 1997.

Appendix A : Uncertainty Analysis for ZnO Kinetics Study

The uncertainty interval that we ascribe to the ZnO decomposition kinetic equation is based on our estimate of the magnitude of errors in the measured independent variables. Table 1A shows the relative uncertainty or uncertainty in each measurement for each error source at a confidence level of 95%. We list the typical sources for measurement errors. Temperature measurements often contain a system disturbance error and a sensor system error. With the PSI-FAMP and the solar blind temperature methods, however, the relative magnitude of energy exchange between the sensor and the system is too low to alter the sample's temperature. We estimate negligible interaction between the sample and sensor that induces an error into the sensor.

Source		Estimated uncertainty intervals at 95 % confidence for the measured variables			
		$+\frac{\delta T}{T}$	$\pm\delta \Delta m$ in g	$\pm\frac{\delta t}{t}$	$\pm\delta D$ in m
Sensor calibration error	Fixed	0.037	0.003		
	Stochastic	0.004	0.0045	0.028	0.0001
Process unsteadiness		0.014			0.0003
Conceptual error		0.022 (Spatial gradients)			

Table 1A: Estimated uncertainty in measurements at a confidence interval of 95%.

The calibration error for the temperature measurement is also given in Schubnell and Tschudi, 1995.* For FAMP there are two components. One is a stochastic error associated with a curve fitting routine. The second error is a non corrected fixed error between a standard and the temperature measured by FAMP. This error was estimated from data presented in (Schubnell and Tschudi, 1995) where FAMP's indicated temperature was compared to that of a reading from an optical pyrometer with a reported fixed error. The calibration errors for the other measurements were taken from manufacturer's literature for the measuring instrument.

The unsteady nature of the process is an error source for the temperature measurement. Random changes in the solar intensity during the course of the experiments accounts for most of this unsteady behaviour. Table 1A shows the typical value from multiple experiments.

It was not possible to readily measure the spatial distribution of the sample's temperature. Nonetheless we acknowledge it as an important error source. The solar flux on the sample is not perfectly uniform. The temperature is thus not perfectly uniform. We estimate the error in our temperature measurement associated with temperature spatial gradients from the flux plot assuming that the solar flux concentration is proportional to the temperature to the fourth power.

These individual measurement errors are propagated to the uncertainty interval that we wish to ascribe to the rate equation with the classical Root Sum Square Method. Our propagation technique is known as the method of sequential perturbation. Figure 1A illustrates the concept. Using the nominal data, a base case computer run establishes an expression for the mass flux as a function of temperature. Three base mass flux values are calculated for three temperatures arbitrarily selected as low, middle and upper values for which we expect the equation to be used in a given application. For estimating the random error component, loop one redoes the above calculation, but the first temperature measurement is perturbed by its uncertainty. The difference between the mass flux for the three arbitrary temperatures and the base case mass flux is squared and stored. The first temperature is then restored to its original value. The next measurement is perturbed and the procedure of establishing a difference between the base case and the perturbed value is again

squared and stored. This procedure is repeated for all measured variables. The total random component of the uncertainty in the mass flux equation associated with the temperature measurement is then the square root of the sum of all the stored differences.

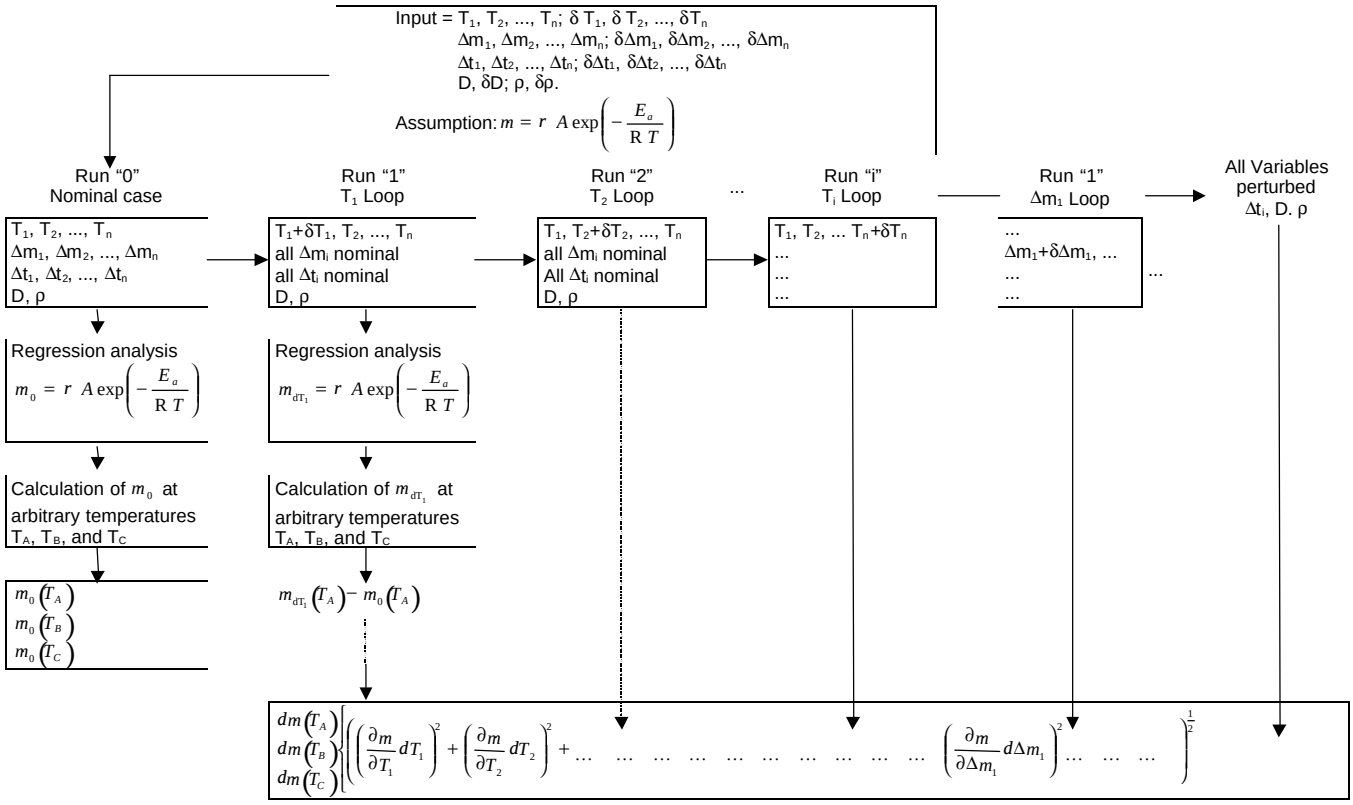

Figure 1A: Uncertainty Analysis via sequential perturbation. (See reference [13]).

This procedure is repeated to estimate the uncertainty in the equation from mass, diameter, and temperature spatial errors. The fixed errors on a measurement are propagated to the equation by perturbing all the data by the fixed error and calculating the new mass flux and comparing the value to the base case. The relative importance of each measurement on the final equation can be seen in Table 2A. Further in depth discussion of the uncertainty analysis is found in ref. [13].

Results: $\dot{m}=1.356 \cdot 10^{9}\ \mathrm{g \cdot m^{-2} \cdot s^{-1}} \exp\left(-\frac{328{,}500}{8.314T}\right) \pm$	Temp. in K	uncertainty in %
	2150	62
	2050	68
	1980	72

Contribution of a measured uncertainty to the uncertainty in mass calculation		
Source	Temperature in K	Uncertainty in %
Temperature Total Random [1)]	2150	16
	2050	25
	1980	33
Temperature Gradients	2150	15
	2050	22
	1980	29
Random error in Δm, D and t	2150	1.1
	2050	1.5
	1980	1.9
Regression analysis[1)]		33
Fixed mass error[1)]	2150	0.07
	2050	0.10
	1980	0.12
Fixed temperature error[1)]	2150	49
	2050	52
	1980	54

[1)] Used to calculate total uncertainty interval

Table 2A: Uncertainty in mass flux equation at a 95% confidence interval for various combinations of measurement errors.

*Schubnell, M. and Tschudi, H. R. (1995) Simultaneous measurement of irradiation, temperature, and reflectivity on hot irradiated surfaces. *Appl. Phys. A,* **60**, 581-587.

Appendix B : Finite Difference Model of ZnO Decomposition:
Combining reaction kinetics and heat transfer

Our approach was to develop a model where we approximated the following physical situation: a reaction taking place under concentrated solar energy principally on a surface of a ZnO slab, a uniform surface temperature, conduction into the slab in one geometric dimension, and a steady state reaction with respect to the decomposition rate. Specifically, the numerical model was used to calculate Zn production rates and the steady-state and unsteady state-temperature profiles within the ZnO under conditions similar to those of solar experiments. The calculated results were compared with those obtained experimentally in order to identify semi-quantitatively how well we understand the underlying physical processes of the rate of thermal dissociation, radiation absorption, and thermal conduction.

The model treats the ZnO as a semi-infinite solid with a solar flux impinging on its front surface. Figure 1B shows that the solid would be continuously fed to the focal point of a solar furnace. The decomposition is presumed to take place only at the ZnO surface. Our model neglects the extent to which the reaction takes place within the ZnO volume, and thus only approximately describes the real situation. We also negelect radiant transport into the solid. However, we forced this physical situation to some extent by working with dense ZnO. Thus any reaction taking place within the ZnO solid volume would experience gas phase mass transfer resistance, which would tend to block the reaction. The gas phase products leaving the front surface, by contrast, are assumed to leave the solid at the place of formation without confronting a resistance to mass transfer and without further heat transfer. Any important gas phase mass transfer resistance that may exist during an experiment will thus influence the values of the experimentally determined kinetic parameters in the decomposition rate equation.

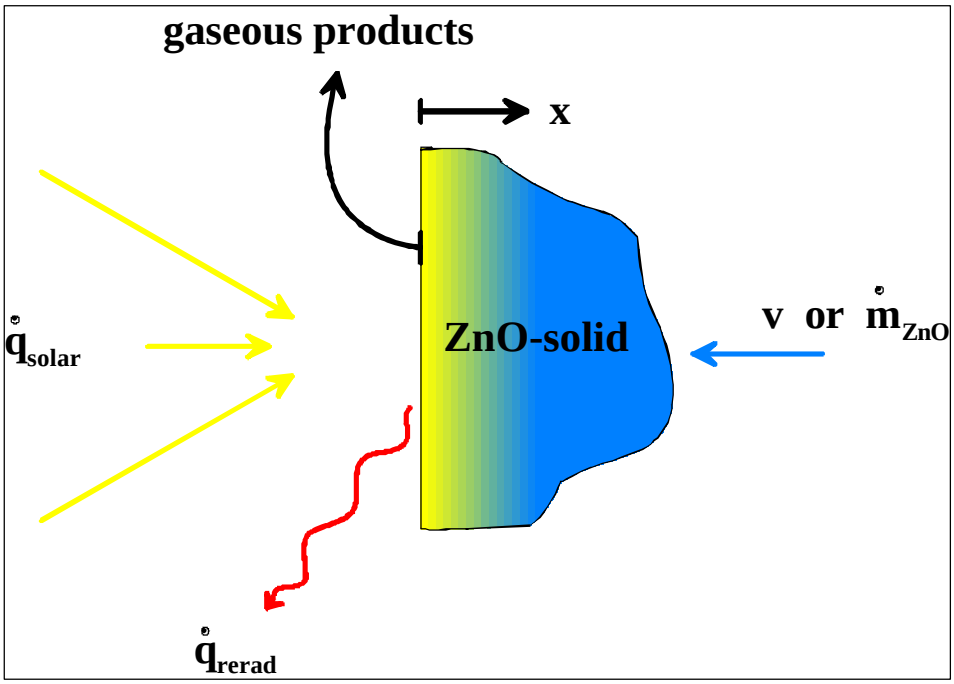

Figure 1B: Model of a surface reaction for a semi-infinite slab of ZnO irradiated with $\dot{q}_{solar}$ on the surface which reradiates to the surrounding with $\dot{q}_{rerad}$. The absorbed energy is both conducted into the solid and used to drive the decomposition reaction.

To simplify the calculation, we assume that the solid ZnO has constant properties. Heat transfer is by radiation on the front surface, $\dot{q}_{solar}$, and it is by conduction in the x-direction within the solid. Heat loss is only by radiation, $\dot{q}_{rerad}$, from the front surface. Under these conditions, ZnO is fed to the focal point of a solar furnace at a velocity *v* so that the decomposing front surface at x = 0 is stationary with respect to absolute co-ordinates.

The reaction rate is assumed to obey an Arrhenius type law:

$$\Re = A \cdot \exp\left(- \frac{E_a}{R \cdot T_s} \right) \tag{1}$$

R is the universal gas constant in J mol^{-1} K^{-1} , T_s represents the surface temperature of the ZnO, A is the apparent pre-exponential factor in g s^{-1} m^{-2}, and E_a is the apparent activation energy in J mol^{-1}.

Conservation of mass at constant density requires

$$\rho \frac{\delta v}{\delta x} = 0 \tag{2}$$

where *v* is the local absolute decomposition velocity of ZnO in the negative x-direction, and ρ is the ZnO density.

In our case, the velocity at x = 0 is such that the mass flux of solid ZnO is exactly balanced by the rate at which it decomposes. Thus ,

$$v = - \frac{\Re}{\rho} \tag{3}$$

The one dimensional energy equation per unit volume applied to a control volume fixed in space is,

$$\rho \cdot c \cdot \frac{\partial T}{\partial t} = - k \frac{\partial^2 T}{\partial x^2} + \rho \cdot v \cdot c \cdot \frac{\partial T}{\partial x} \cdot \tag{4}$$

The first term is the rate at which energy is stored in the solid per unit volume. The remaining terms describe the net thermal energy by conduction per unit volume into a differential control volume and the convective transport of energy into the same control volume.

The boundary conditions for equations 3 and 4 are

$$-k \cdot \left. \frac{\partial T}{\partial x} \right|_{x=0} = \alpha \cdot q_{solar} - \varepsilon \cdot \sigma \cdot T^4 (x=0) \quad - \Re \cdot \Delta H_{rxn} \tag{5}$$

$$T|_{x=\infty} = 300 K \tag{6}$$

T = 300 K @ *t* = 0 seconds. (7)

Equation 5 states that the energy flux conducted into the ZnO solid is the difference between the absorbed solar energy and the energy radiated to the environment and the energy flux leaving the surface due to the vaporization of ZnO(s) to its elements.